INTERNATIONAL JOURNAL OF AUTOMOTIVE AND MECHANICAL ENGINEERING (IJAME)
ISSN: 2229-8649 e-ISSN: 2180-1606
VOL. XX, ISSUE XX, XXX – XXX
DOI: https://doi.org/10.15282/ijame.v#i#.###

ORIGINAL ARTICLE

Driving into the Dynamics–Leveraging the Direct-Quadrature-Zero Transform for Mechanical Systems

José M. Campos-Salazar [1]*, Juan L. Aguayo-Lazcano [2], Roya Rafiezadeh[3]

[1] Electronic Engineering Department, Universitat Politècnica de Catalunya, Barcelona, Spain
[2] Institute of Physical and Mathematical Sciences, Universidad Austral de Chile, Valdivia, Chile
[3] Power Electronics, Machines and Control, University of Nottingham, United Kingdom

ABSTRACT – This research offers a thorough analysis of the dynamic behavior of 1, 2, and 3-degrees-of-freedom (DoF) mechanical systems under a sinusoidal force, examining both mechanical and dq coordinates. By utilizing standardized initial conditions, the 1-DoF system displays fascinating oscillatory patterns with dual frequency components, highlighting the significance of low damping. The adaptation to dq coordinates simplifies the analysis and highlights the system's nuanced behavior. In contrast, the 2-DoF system exhibits intricate interactions, oscillation phenomena, and multiple frequency components in mechanical coordinates. The contribution of masses that do not experience external forces in dq coordinates is minimal. On the other hand, the 3-DoF system shows diverse interactions and frequency components that are different from the dq transformations. The observed dynamics not only enhance comprehension of these systems but also provide valuable insights for refining analytical approaches in the analysis of dynamic systems. This study sets the stage for future investigations and urges the development of streamlined analytical frameworks for a more focused exploration of externally influenced variables in dynamic mechanical systems.

ARTICLE HISTORY
Received: xxxx
Revised: xxxx
Accepted: xxxx
Published: xxxx

KEYWORDS
Dynamic analysis
DQ coordinates
Multi-DOF systems
Mechanical system
Dynamics

1.0 INTRODUCTION

Vibration analysis is a fundamental area within mechanical engineering that focuses on examining the oscillatory behavior of mechanical systems subjected to external excitations, such as forces or displacements [1]. The ability to analyze vibrations is essential across multiple industries, including manufacturing [2]–[6], automation [7]–[10], and aerospace [11], [12], as it provides crucial insights into system performance, safety, and longevity. This field plays a pivotal role in designing, optimizing, and maintaining mechanical systems by identifying and mitigating vibrational effects that could lead to structural failures or inefficiencies.

One of the key challenges in vibration analysis is the complexity introduced by various factors such as frequency, damping characteristics, and system interactions. The study in [2] underscores the necessity of addressing these challenges through advanced methodologies, including modal analysis, Fourier transforms, wavelet-based techniques, and computational simulations. By leveraging such methods, engineers can gain a deeper understanding of vibrational phenomena and develop strategies to enhance the performance of mechanical systems.

A review in [3] explores vibration-based diagnostic techniques for identifying rolling bearing failures in industrial machinery. Given the broad range of operational conditions and failure modes, precise fault detection is critical to ensuring system reliability. The study evaluates multiple vibration analysis methods, including time-domain, frequency-domain, and time-frequency-domain approaches, emphasizing their role in predictive maintenance and minimizing downtime.

Similarly, research on process plants, as discussed in[4], highlights the significance of effective machine management in preventing costly operational disruptions. The study explores the implementation of condition monitoring and preventive maintenance strategies, demonstrating the effectiveness of vibration analysis in early fault detection. Through practical case studies, the study illustrates how dynamic vibration analysis can accurately diagnose mechanical irregularities before they lead to critical failures.

The work in [5] focuses on fundamental vibration concepts, particularly for single-degree-of-freedom mechanical systems. It presents a structured approach to analyzing dynamic behaviors in these systems, laying the foundation for studying more complex mechanical structures. The study covers essential topics such as system response to harmonic excitation, transient behavior, and resonance effects, reinforcing the importance of vibration analysis in engineering design and maintenance.

The role of vibration analysis extends to the automotive industry, where it is crucial for enhancing vehicle stability,

*CORRESPONDING AUTHOR | J. M. Campos-Salazar | ✉ jose.manuel.campos@upc.edu

safety, and passenger comfort. The study in [6] discusses active vibration control techniques, emphasizing their role in mitigating the negative effects of oscillatory motion in vehicles. The research explores cutting-edge control methodologies designed to optimize vehicle performance and reduce driver discomfort caused by excessive vibrations.

An experimental investigation in [7] further explores the intricate relationship between vehicle maintenance and mechanical vibrations. The study demonstrates how inadequate maintenance can lead to increased vibrations and, subsequently, mechanical failures. Advanced sensor-based data acquisition techniques, including signal processing methods such as fast Fourier transform, are employed to analyze and control vibrations. The research underscores the importance of predictive maintenance in prolonging vehicle lifespan and ensuring operational efficiency.

In the context of mechanical transmission systems, the study in [8] examines strategies for mitigating torsional vibrations in automotive applications. Effective torsional vibration control is critical for ensuring the longevity and optimal performance of transmission components. The study evaluates damping mechanisms, gear optimization techniques, and dynamic balancing strategies, highlighting their significance in enhancing drivetrain efficiency and minimizing frictional losses.

Expanding this perspective, the study in [9] presents a comparative evaluation of various automotive vibration testing methodologies. The research focuses on techniques such as frequency-domain analysis, time-domain analysis, and statistical modeling to assess the reliability of automotive components. These methods are instrumental in refining vehicle designs, improving ride quality, and ensuring adherence to safety standards.

Noise and vibration management in automobiles is another critical topic discussed in [10]. The study addresses the integration of advanced materials, structural optimization, and active noise control strategies to minimize vibration-related disturbances in vehicles. The research highlights the synergy between engineering design and acoustics in developing vehicles with superior noise and vibration characteristics.

In the aerospace sector, vibration analysis plays a crucial role in failure prevention and system reliability. The study in [11] investigates the mechanical simulation of high-reliability aerospace electronics, emphasizing the necessity of vibration testing for ensuring the durability of electronic components. Techniques such as finite element analysis, computational modeling, and experimental validation are employed to predict and mitigate vibrational effects in aerospace environments.

Research in [12] explores vibration suppression in flexible aerospace structures. The study examines innovative approaches such as active disturbance rejection control and frequency-domain techniques to manage vibration-induced challenges in aircraft structures. The findings contribute to the development of more resilient aerospace systems capable of withstanding extreme operational conditions.

As mechanical systems increase in complexity, the challenges associated with vibration analysis also grow [1]. The study in [13] investigates lateral vibration dynamics in transportation applications, highlighting the difficulties in predicting and analyzing structural responses under variable loading conditions. Advanced computational methods are essential for designing transportation systems that can endure vibrational stresses while maintaining structural integrity.

The intersection of vibration analysis and reliability engineering is explored in [14], which examines the effects of vibrational fatigue on mechanical components. The study emphasizes the importance of accurately modeling the interaction between fatigue and dynamic forces to improve system reliability. By understanding these interactions, engineers can develop robust mechanical designs that resist premature failures.

The book in [15] presents an in-depth discussion of modeling techniques for vibrational fatigue and structural fracture analysis. It highlights the complexities associated with predicting fatigue life under dynamic loading conditions, taking into account factors such as material properties, environmental influences, and resonance phenomena. The study underscores the importance of integrating computational models that accurately reflect real-world vibrational behaviors.

In [16], a comprehensive review of vibration analysis techniques for rotating machinery is presented, focusing on predictive maintenance applications. The study compares traditional methods, such as time-domain and frequency-domain analysis, with emerging AI-based approaches, including neural networks and support vector machines. The findings highlight the growing role of artificial intelligence in enhancing fault detection and machine diagnostics.

The study in [17] explores prediction methods for transient vibration and sound radiation in structural plates. It evaluates conventional approaches, such as finite element analysis and boundary element methods, as well as novel wave-based techniques. The research provides valuable insights into optimizing structural designs for improved vibration and acoustic performance.

The research in [18] examines the use of non-traditional dynamic vibration absorbers for mitigating vibrations in damped linear structures. By leveraging advanced damping technologies, the study proposes innovative solutions for controlling structural vibrations in diverse engineering applications.

A broader examination of machine diagnostics through vibration analysis is provided in [19]. The study discusses the integration of artificial intelligence techniques, such as fuzzy logic and genetic algorithms, to enhance fault detection capabilities in industrial machinery. The findings highlight the potential of AI-driven solutions in predictive maintenance.

The study in [20] conducts a modal analysis of the Karun-4 concrete arch dam, utilizing a finite element model (FEM) to assess the dynamic behavior of the dam-reservoir-foundation system. To validate the computational model, the authors compare the FEM results with ambient vibration test data. The analysis investigates the influence of several critical factors, including reservoir water levels, foundation rock mass properties, and seismic excitations, on the natural frequencies and mode shapes of the structure. The findings reveal that reservoir water levels significantly impact the modal properties of the dam, while the foundation rock mass exhibits only minor effects. In contrast, earthquake-induced

excitation has a negligible influence on the dam's dynamic response. Based on these results, the study concludes that the proposed FEM approach is a reliable tool for evaluating the structural dynamics of large-scale hydraulic infrastructures.

The study in [21] explores modal analysis, a fundamental technique for examining the dynamic characteristics of mechanical structures and systems. The authors provide an extensive review of testing methodologies and system identification techniques, highlighting their role in characterizing vibrational responses. Additionally, the paper addresses key practical challenges encountered in modal analysis, along with emerging trends that enhance its application in structural dynamics. To reinforce these concepts, the study incorporates case studies that illustrate real-world implementations of modal analysis techniques. This work serves as a valuable reference for researchers and engineers seeking deeper insights into vibration-based structural assessment and system behavior characterization.

From the literature review, it is evident that existing vibration analysis methods predominantly focus on frequency-domain, time-domain, and AI-based techniques. However, these approaches often face limitations when applied to vibrational systems with continuously varying states, particularly in cases involving sinusoidal oscillations. Traditional control strategies struggle to regulate such systems effectively due to the dynamic nature of the variables involved [22]–[24].

A promising alternative is the application of coordinate transformations to simplify the analysis of oscillatory systems. The direct-quadrature-zero (dq0) transformation provides a means of converting time-varying system states into a rotating reference frame, facilitating more efficient modeling and control [25]. Despite its widespread use in electrical engineering, there is a notable absence of studies applying the dq0 transformation to mechanical vibration analysis.

To address this gap, this study investigates the application of the dq0 transformation to mechanical vibrational systems with one, two, and three degrees of freedom. The research develops dynamic models for these systems in both the natural mechanical frame and the transformed dq0 frame, enabling a comparative evaluation of their vibrational characteristics.

This study is primarily theoretical and aims to validate the suitability of dq0 transformation-based models for mechanical vibration analysis. The remainder of the paper is structured as follows: Section 2 presents the mathematical formulation of the Park and Clarke transformations, while Section 3 discusses the application of the dq0 transformation to mechanical vibrational systems. Section 4 introduces energy equations relevant to the studied systems, and Section 5 derives the state-space representations of the models. Simulation results are presented in Section 6, followed by the conclusions in Section 7.

2.0 ANALYSIS OF ROTATIONAL REFERENCE FRAME TRANSFORMATIONS

The study of reference frame transformations, particularly the Clarke (αβ0) and Park (dq0) transformations, plays a crucial role in electrical engineering, especially in the control and analysis of three-phase systems [26]–[30]. These mathematical frameworks enable the conversion of three-phase variables—such as currents and voltages—from the natural *abc* coordinate system to alternative domains that simplify modeling and control. The *abc* reference frame represents three-phase electrical quantities as sinusoidal signals with a phase shift of 120°, which, while fundamental to power systems, is not always the most computationally efficient framework for dynamic system analysis. For applications in motor drives, power converters, and grid-interfaced systems, it is often advantageous to transform these variables into a more structured and computationally manageable reference frame.

The Park transformation (dq0) introduces a rotating coordinate system that follows a specific reference, such as the magnetic field in an electric machine or the voltage vector of an inverter. This transformation segregates three-phase components into two orthogonal axes: the direct axis (d-axis), which aligns with active power, and the quadrature axis (q-axis), associated with reactive power. A third component, the zero-sequence term, represents any unbalanced or neutral-point voltage variations [25]. Meanwhile, the Clarke transformation (αβ0) acts as an intermediary step, projecting three-phase signals onto a stationary two-axis system, where the α- and β-axes provide an equivalent representation of the three-phase system in a simplified orthogonal framework.

The relationship between these two transformations is dictated by a rotational transformation matrix. The Clarke transformation first maps *abc* variables into the stationary αβ0 frame, and then the Park transformation further rotates these quantities into the dq0 frame, which follows the motion of the machine or inverter system [25]. The rotation angle of the dq0 transformation corresponds to the angular position or frequency of the rotating system, allowing for an effective dynamic representation of electrical variables in a more tractable form.

Beyond mere mathematical convenience, these transformations provide significant benefits in real-world applications. By converting three-phase systems into equivalent two-phase representations, they simplify complex differential equations governing electromechanical dynamics, thereby reducing computational overhead in real-time control applications. Moreover, they facilitate independent control over active and reactive power, forming the basis of advanced control methodologies such as field-oriented control (FOC) and direct torque control (DTC) in electrical machines. These methods enhance precision in regulating parameters like torque, flux, voltage, and current, leading to improved efficiency in motor drives, power electronics, and grid-tied inverters [25].

In summary, the Clarke and Park transformations serve as essential mathematical tools that bridge the *abc* reference frame with the αβ0 and dq0 domains. Their ability to simplify system dynamics, improve analytical tractability, and enhance control implementations makes them indispensable in power electronics, motor control, and grid-interfaced applications. Their broad adoption underscores their fundamental role in improving stability, efficiency, and performance in three-phase electrical systems.

2.1 Derivation of the Clarke Transformation Matrix

The Clarke transformation provides a powerful method for re-expressing three-phase electrical variables in an alternative coordinate system that simplifies analysis and control. By mapping the *abc* reference frame to a two-axis αβ0 reference frame, this transformation effectively decouples three-phase interactions and provides a clearer representation of system behavior. One key advantage is its ability to isolate the common-mode, or zero-sequence, component, which accounts for any unbalanced neutral currents or common-mode voltages [25], [31]. The αβ0 transformation ensures energy conservation, follows the right-hand coordinate system convention, and maintains uniform scaling properties, making it indispensable for applications such as power conversion, motor drives, and grid-connected electronics [25], [31].

The transformation matrix used for Clarke's transformation, denoted as $\mathbf{K_C}$, is formulated as a power-invariant, right-handed transformation:

$$\mathbf{K_C} = \sqrt{\frac{2}{3}} \cdot \begin{bmatrix} 1 & -\frac{1}{2} & -\frac{1}{2} \\ 0 & \frac{\sqrt{3}}{2} & -\frac{\sqrt{3}}{2} \\ \frac{1}{\sqrt{2}} & \frac{1}{\sqrt{2}} & \frac{1}{\sqrt{2}} \end{bmatrix} \tag{1}$$

Applying this transformation to a three-phase column vector, $m_{abc}(t)$, produces the corresponding vector in the αβ0 domain:

$$\mathbf{m_{\alpha\beta0}}(t) = \mathbf{K_c} \cdot \mathbf{m_{abc}}(t) \tag{2}$$

To revert to the original *abc* frame, the inverse transformation is applied:

$$\mathbf{m_{abc}}(t) = \mathbf{K_c}^{-1} \cdot \mathbf{m_{\alpha\beta0}}(t) \tag{3}$$

This bidirectional transformation capability ensures that the αβ0 transformation preserves the fundamental properties of the system while simplifying control equations. The Clarke transformation is particularly beneficial in vector control strategies, as it provides an effective means of analyzing three-phase systems in a reduced-dimensional space, improving control response and computational efficiency.

2.2 Derivation of the Park Transformation

The Park transformation, also known as the dq0 transformation, is another fundamental tool used to convert stationary αβ0 coordinates into a rotating reference frame that aligns with system dynamics [25], [31]. Widely applied in power electronics, motor control, and grid-connected systems, this transformation enables precise tracking and control of three-phase variables. The primary feature of the Park transformation is its ability to "rotate" the reference frame to align with a desired frequency, typically the synchronous frequency of an electrical machine. This results in a transformation where sinusoidal variables in the αβ0 domain become dc quantities in the dq0 frame, greatly simplifying system control.

A key advantage of the dq0 transformation is its ability to modify the frequency spectrum of a signal. By aligning the transformation reference frame with a system's synchronous frequency, it converts fundamental-frequency components into steady-state dc values, while components at different frequencies appear as ac variations. This is particularly valuable for control methodologies such as field-oriented control (FOC), where separating active and reactive power components is critical for efficient motor and converter operation [25], [31].

Mathematically, the Park transformation matrix is expressed as:

The dq0 transformation is defined mathematically using the transformation matrix $\mathbf{K_P}$, given by:

$$\mathbf{K_P} = \begin{bmatrix} \cos\theta(t) & \sin\theta(t) & 0 \\ -\sin\theta(t) & \cos\theta(t) & 0 \\ 0 & 0 & 1 \end{bmatrix} \tag{4}$$

where $\theta(t)$ represents the instantaneous angular position of the reference frame. Applying this transformation to an αβ0 column vector results in:

$$\mathbf{m_{dq0}}(t) = \mathbf{K_P} \cdot \mathbf{m_{\alpha\beta0}}(t) \tag{5}$$

To return to the αβ0 frame, the inverse transformation is applied:

$$\mathbf{m_{\alpha\beta 0}}(t) = \mathbf{K_P}^{-1} \cdot \mathbf{m_{dq0}}(t) \tag{6}$$

Alternatively, the transformation can be applied directly from the *abc* frame using the combined Clarke-Park transformation matrix: $\mathbf{K_{CP}} = \mathbf{K_C} \cdot \mathbf{K_P}$. The resulting transformation matrix is expressed as:

$$\mathbf{K_{CP}} = \sqrt{\frac{2}{3}} \cdot \begin{bmatrix} \cos\theta(t) & \cos\left(\theta(t) - \frac{2\cdot\pi}{3}\right) & \cos\left(\theta(t) + \frac{2\cdot\pi}{3}\right) \\ -\sin\theta(t) & -\sin\left(\theta(t) - \frac{2\cdot\pi}{3}\right) & -\sin\left(\theta(t) + \frac{2\cdot\pi}{3}\right) \\ \frac{\sqrt{2}}{2} & \frac{\sqrt{2}}{2} & \frac{\sqrt{2}}{2} \end{bmatrix} \tag{7}$$

The inverse transformation matrix, used to return from the dq0 reference frame back to the *abc* reference frame, is given by:

$$\mathbf{K_{CP}} = \sqrt{\frac{2}{3}} \cdot \begin{bmatrix} \cos\theta(t) & \cos\left(\theta(t) - \frac{2\cdot\pi}{3}\right) & \cos\left(\theta(t) + \frac{2\cdot\pi}{3}\right) \\ -\sin\theta(t) & -\sin\left(\theta(t) - \frac{2\cdot\pi}{3}\right) & -\sin\left(\theta(t) + \frac{2\cdot\pi}{3}\right) \\ \frac{\sqrt{2}}{2} & \frac{\sqrt{2}}{2} & \frac{\sqrt{2}}{2} \end{bmatrix} \tag{7}$$

The direct transformation from *abc* to dq0 can be defined as:

$$\mathbf{m_{dq0}}(t) = \mathbf{K_{CP}} \cdot \mathbf{m_{abc}}(t) \tag{9}$$

The inverse transformation allows conversion back to the *abc* reference frame:

$$\mathbf{m_{abc}}(t) = \mathbf{K_{CP}}^{-1} \cdot \mathbf{m_{dq0}}(t) \tag{10}$$

The dq0 transformation is fundamentally rooted in vector projections and rotational transformations within a Cartesian coordinate system [25], [31]. To conceptualize this, imagine both the αβ and dq coordinate frames being displayed simultaneously, as illustrated in **Figure 1**. The vector $\mathbf{m}_{\alpha\beta}(t)$, originally expressed in the αβ reference frame, undergoes a transformation as the dq reference frame rotates by an angle $\theta(t)$ with respect to the fixed αβ frame.

Mathematically, in Cartesian notation, a vector within the αβ frame can be represented as:

$$\mathbf{m_{\alpha\beta}}(t) = \mathbf{m_\alpha}(t) \cdot \hat{\mathbf{u}}_\alpha + \mathbf{m_\beta}(t) \cdot \hat{\mathbf{u}}_\beta \tag{11}$$

where $\hat{\mathbf{u}}_\alpha$ and $\hat{\mathbf{u}}_\beta$ are the unit basis vectors of the stationary αβ reference frame. The dq frame, being a rotated version of the αβ frame, establishes a new orientation defined by $\theta(t)$, where $\hat{\mathbf{u}}_\alpha$ and $\hat{\mathbf{u}}_\mathbf{d}$ serve as its respective unit vectors [25], [31]. The transformation linking these coordinate frames is given by:

$$\begin{cases} \hat{\mathbf{u}}_\mathbf{d} = \cos\big(\theta(t)\big) \cdot \hat{\mathbf{u}}_\alpha + \mathbf{sin}\big(\theta(t)\big) \cdot \hat{\mathbf{u}}_\beta \\ \hat{\mathbf{u}}_\mathbf{q} = -\mathbf{sin}\big(\theta(t)\big) \cdot \hat{\mathbf{u}}_\alpha + \mathbf{cos}\big(\theta(t)\big) \cdot \hat{\mathbf{u}}_\beta \end{cases} \tag{12}$$

Applying the dot product to project the αβ components onto the dq axes results in:

$$\begin{cases} \mathbf{m_d}(t) = \hat{\mathbf{u}}_\mathbf{d} \cdot \mathbf{m_{\alpha\beta}}(t) = \cos\big(\theta(t)\big) \cdot \mathbf{m_\alpha}(t) + \sin\big(\theta(t)\big) \cdot \mathbf{m_\beta}(t) \\ \mathbf{m_q}(t) = \hat{\mathbf{u}}_\mathbf{q} \cdot \mathbf{m_{\alpha\beta}}(t) = -\sin\big(\theta(t)\big) \cdot \mathbf{m_\alpha}(t) + \cos\big(\theta(t)\big) \cdot \mathbf{m_\beta}(t) \end{cases} \tag{13}$$

These transformed components, md(t)m_d(t)md(t) and mq(t)m_q(t)mq(t), form the new representation of the original vector in the dq reference frame. One important characteristic of this transformation is that a positive θ(t)\theta(t)θ(t) corresponds to a counterclockwise rotation, effectively shifting the vector's angular representation in the dq domain. This property is particularly useful in three-phase electrical systems, where rotating reference frames track system variables in synchrony with fundamental electrical frequencies, ensuring that transformed dq components appear as stationary values in the new coordinate system [25], [31].

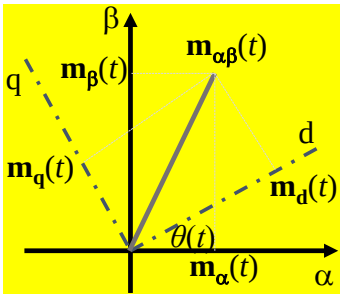

Figure 1. Geometric representation of an arbitrary vector $\mathbf{m}_{\alpha\beta}(t)$ in reference frames αβ and dq. In addition, the vector components of the vector in its two reference frames are included [32]

These components, $\mathbf{m}_{d}(t)$ and $\mathbf{m}_{q}(t)$, constitute the transformed vector $\mathbf{m}_{dq}(t)$ in the dq reference frame. Notably, the positive angle $\theta(t)$ corresponds to a counterclockwise rotation, effectively reducing the vector's angle in the new dq frame. This is due to the fact that the reference frame itself undergoes a forward rotation rather than the vector itself. As a result, in scenarios such as three-phase electrical systems, where the reference frame rotates forward, the transformed dq vector remains stationary in the new coordinate system [25], [31].

From a matrix formulation perspective, the conversion between αβ and dq coordinates relies on a structured transformation matrix. The corresponding transformation matrix $\mathbf{K_P}$ is defined as:

$$\mathbf{K_P} = \begin{bmatrix} \cos\theta(t) & \sin\theta(t) \\ -\sin\theta(t) & \cos\theta(t) \end{bmatrix} \tag{14}$$

which establishes the following relationship: $\mathbf{m}_{dq}(t) = \mathbf{K_P} \cdot \mathbf{m}_{\alpha\beta}(t)$. This representation facilitates a direct mathematical mapping between the stationary αβ and rotating dq coordinate systems, providing a streamlined framework for dynamic system analysis and control.

While the dq0 transformation is typically applied to three-phase systems, a similar approach can be utilized for single-phase signals. In such cases, directly applying the transformation defined in (9) may not be straightforward due to the absence of a naturally occurring quadrature component. To circumvent this, a modified Clarke transformation can be introduced, which generates an auxiliary 90-degree phase-shifted signal, enabling an equivalent two-phase representation. This adaptation follows the transformation:

$$\begin{cases} \mathbf{m}_{\alpha}(t) = \mathbf{m}_{\mathbf{a}}(t) \\ \mathbf{m}_{\beta}(t) = \mathbf{m}_{\mathbf{a}}\left(t - \frac{\pi}{2}\right) \end{cases} \tag{15}$$

Here, $\mathbf{m}_{\alpha}(t)$ retains the original signal, while $\mathbf{m}_{\beta}(t)$ represents a derived quadrature-phase component. Once mapped into the αβ coordinate system, the standard dq0 transformation defined by $\mathbf{K_P}$ can be applied, allowing single-phase signals to be analyzed and controlled in a similar manner to three-phase systems [25], [31].

3.0 APPLICATION OF THE PARK TRANSFORMS INTO A DYNAMIC VIBRATIONAL MECHANICAL SYSTEM

This section presents a comprehensive mathematical examination of the dq0 transformation method applied to vibrational mechanical-dynamical systems. The analysis encompasses three distinct configurations: one-degree-of-freedom (1-DoF), two-degree-of-freedom (2-DoF), and three-degree-of-freedom (3-DoF) systems, as illustrated in **Figure 2(a)**, **(b)**, and **(c)**, respectively.

Each system is uniquely characterized by a set of dynamic parameters, including mass (m_i), stiffness (k_i), and damping (b_i), where $i \in \{1,2,3\}$. These parameters define the structural and vibrational behavior of the system under external excitation. Notably, the mass elements (m_i) are assumed to be rigid and inelastic, remaining fixed to immovable reference structures to ensure idealized vibrational analysis [34].

The simplest configuration, depicted in **Figure 2(a)**, consists of a single mass element (m_1) connected to a stationary wall via a spring-damper system composed of a stiffness element (k_1) and a damping element (b_1). This system exhibits classical harmonic oscillation, serving as a foundational model for analyzing mechanical vibrations.

The two-degree-of-freedom (2-DoF) system, illustrated in **Figure 2(b)**, introduces an additional mass element (m_2), resulting in a more complex vibrational interaction. In this configuration:

- m_1 remains connected to the stationary wall through elements k_1 and b_1.
- m_1 is also coupled to m_2 via intermediate stiffness (k_2) and damping (b_2) elements.

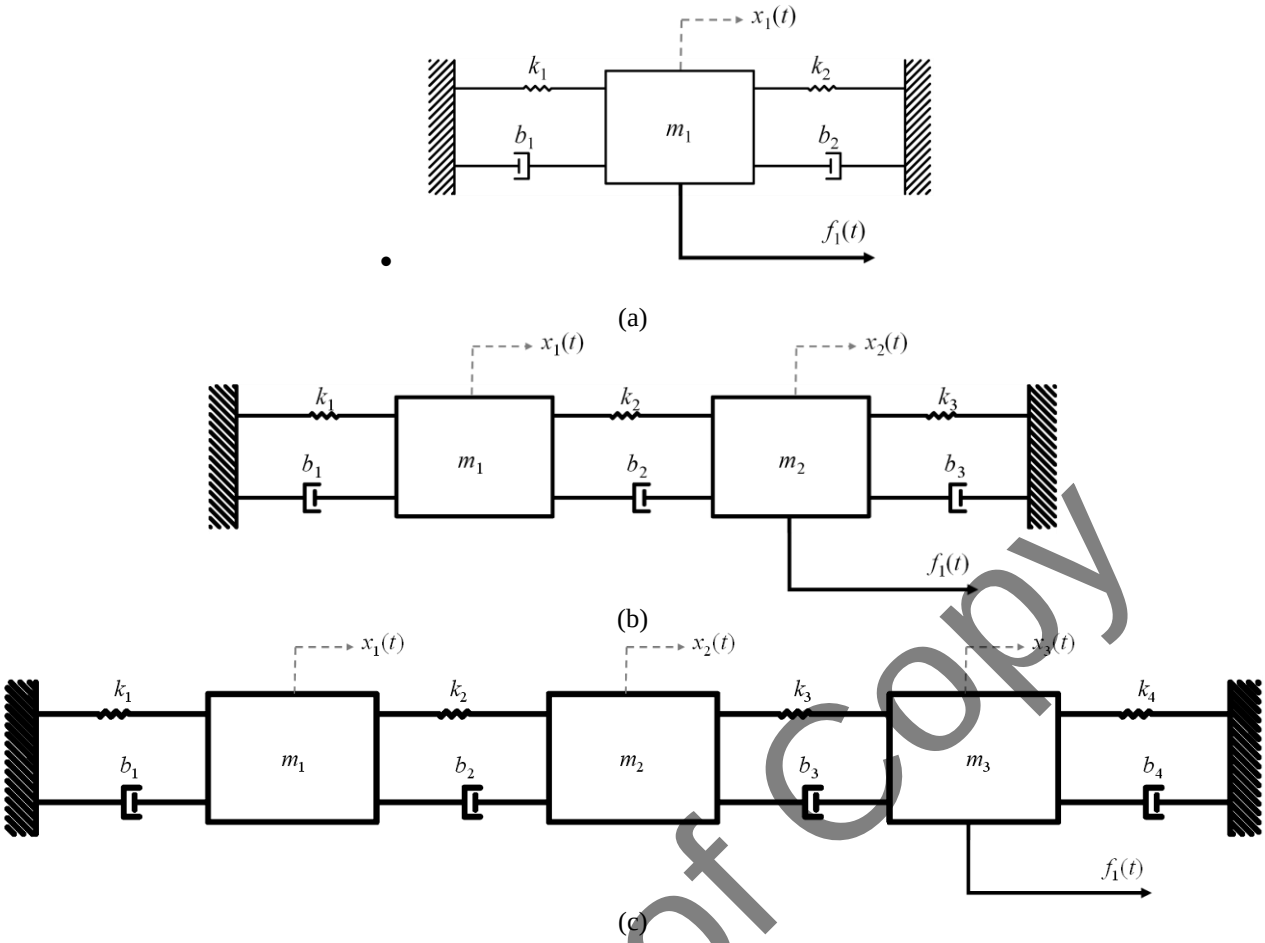

Figure 2. Proposed vibrational mechanical dynamic models to which dq0 will be applied. (a) 1-DoF. (b) 2-DoF. (c) 3-DoF

This arrangement introduces coupled oscillatory behavior, where energy exchange between m_1 and m_2 leads to modal interactions that significantly influence the system's dynamic response.

The three-degree-of-freedom (3-DoF) system, depicted in **Figure 2(c)**, further extends the complexity of vibrational interactions by incorporating a third mass element (m_3). The structure is defined as follows:

- m_1 is anchored to the stationary wall via k_1 and b_1.
- m_1 and m_3 are each connected to m_2 through additional coupling elements (k_2, b_2) and (k_3, b_3), respectively.

This system introduces multiple degrees of vibrational freedom, leading to higher-order modal interactions and resonance phenomena. The interdependent motion of m_1, m_2, and m_3 results in complex vibrational modes, making it an ideal model for studying multi-body oscillatory dynamics.

The physical units associated with each system parameter are as follows:

- Mass (m_i): Newton (N)
- Stiffness (k_i): Newton per meter (N/m)
- Damping (b_i): Newton-seconds per meter (N·s/m)

The primary dynamic variables governing the system's behavior include the external force $f_1(t)$ and the displacement responses $x_i(t)$, where $i \in \{1,2,3\}$ represents each mass element's positional deviation. The excitation force is mathematically defined as: $f_1(t) = F \cdot \sin(\omega \cdot t)$, where F denotes the force amplitude, and ω represents the angular frequency of excitation. This sinusoidal excitation drives the oscillatory motion of the system, serving as the basis for analyzing vibrational behavior under harmonic forcing conditions.

3.1 Analysis of a Mechanical-Vibrational-Dynamical System of One-Degree-of-Freedom

This section presents a detailed analysis of the 1-DoF vibrational mechanical system, as illustrated in **Figure 2(a)**. The primary objective is to derive the system's energy equations and formulate the Lagrangian equation in terms of generalized coordinates ($p_i(t)$), facilitating the modeling of this non-conservative system [35]. By following this approach,

the dynamic equation of motion for the system in **Figure 2(a)** is obtained. Specifically, expressions for the system's kinetic energy ($KE(t)$), potential energy ($PE(t)$), and dissipation energy ($DE(t)$) are given as follows:

$$\begin{cases} KE(t) = \frac{1}{2} \cdot m_1 \cdot \dot{x}_1(t)^2 \\ PE(t) = \frac{1}{2} \cdot k_{\mathrm{eq}_1} \cdot x_1(t)^2 \\ DE(t) = \frac{1}{2} \cdot b_{\mathrm{eq}_1} \cdot \dot{x}_1(t)^2 \end{cases} \tag{16}$$

From here, the equivalent damping coefficient and stiffness terms are defined as $b_{eq1} = b_1 + b_2$ and $k_{eq1} = k_1 + k_2$, respectively.

The Lagrangian equation for $p_i(t)$ is expressed as:

$$\frac{\mathrm{d}}{\mathrm{d}t}\frac{\partial KE(t)}{\partial \dot{p}_\mathrm{i}(t)} - \frac{\partial KE(t)}{\partial p_\mathrm{i}(t)} + \frac{\partial PE(t)}{\partial p_\mathrm{i}(t)} + \frac{\partial DE(t)}{\partial \dot{p}_\mathrm{i}(t)} = \Psi_\mathrm{i}(t) \tag{17}$$

where $\Psi_1(t)$ represents the generalized external force applied to the system, defined in this case as $\Psi_1(t) = f_1(t)$. Given that $p_1(t) = x_1(t)$, substituting these expressions into the Lagrange equation and applying algebraic manipulations yield the state-space representation of the 1-DoF system:

$$\begin{cases} \frac{\mathrm{d}\mathbf{q}(t)}{\mathrm{d}t} = \mathbf{A} \cdot \mathbf{q}(t) + \mathbf{B} \cdot u(t) \\ \mathbf{y}(t) = \mathbf{C} \cdot \mathbf{q}(t) + \mathbf{D} \cdot u(t) \end{cases} \tag{18}$$

where $q(t)$ and $y(t)$ denote the state vector and output vector, while $u(t)$ represents the scalar input. Specifically: $\mathbf{q}(t) = [q_1(t), q_2(t)]^\mathrm{T}$, where $q_1(t) = x_1(t)$ and $q_2(t) = \mathrm{d}x_1(t)/\mathrm{d}t$, and $u(t) = f_1(t)$. Symbolically, $\{\mathbf{q}(t), \mathbf{y}(t)\} \in \{\mathbb{R}^2\}$. The matrices **A**, **B** are defined as follows

The corresponding system matrices are defined as:

$$\mathbf{A} = \begin{bmatrix} 0 & 1 \\ -\frac{k_{\mathrm{eq}_1}}{m_1} & -\frac{b_{\mathrm{eq}_1}}{m_1} \end{bmatrix} \mathbf{B} = \begin{bmatrix} 0 \\ \frac{1}{m_1} \end{bmatrix} \tag{19}$$

The output (**C**) and direct transmission (**D**) matrices are given as **C** = **I** (identity matrix) and **D** = **0** (zero matrix), respectively. Symbolically, the matrices satisfy: $\{\mathbf{A}, \mathbf{C}\} \in \mathcal{M}_{2x2}$ and $\{\mathbf{B}, \mathbf{D}\} \in \mathcal{M}_{2x1}$.

To facilitate the application of the dq0 transformation, the system is first transformed into the αβ\alpha\betaαβ coordinate frame using the following equivalences:

$$\begin{cases} \frac{\mathrm{d}\mathbf{q}_{\boldsymbol{\alpha\beta}}(t)}{\mathrm{d}t} = \mathbf{A}_{\boldsymbol{\alpha\beta}} \cdot \mathbf{q}_{\boldsymbol{\alpha\beta}}(t) + \mathbf{B}_{\boldsymbol{\alpha\beta}} \cdot \mathbf{u}_{\boldsymbol{\alpha\beta}}(t) \\ \mathbf{y}_{\boldsymbol{\alpha\beta}}(t) = \mathbf{C}_{\boldsymbol{\alpha\beta}} \cdot \mathbf{q}_{\boldsymbol{\alpha\beta}}(t) + \mathbf{D}_{\boldsymbol{\alpha\beta}} \cdot \mathbf{u}_{\boldsymbol{\alpha\beta}}(t) \end{cases} \tag{21}$$

where the matrices in αβ coordinates are:

$$\mathbf{A}_{\boldsymbol{\alpha\beta}} = \begin{bmatrix} 0 & 0 & 1 & 0 \\ 0 & 0 & 0 & 1 \\ -\frac{k_{\mathrm{eq}_1}}{m_1} & 0 & -\frac{b_{\mathrm{eq}_1}}{m_1} & 0 \\ 0 & -\frac{k_{\mathrm{eq}_1}}{m_1} & 0 & -\frac{b_{\mathrm{eq}_1}}{m_1} \end{bmatrix} \mathbf{B}_{\boldsymbol{\alpha\beta}} = \begin{bmatrix} 0 & 0 \\ 0 & 0 \\ \frac{1}{m_1} & 0 \\ 0 & \frac{1}{m_1} \end{bmatrix} \tag{22}$$

The output ($\mathbf{C}_{\boldsymbol{\alpha\beta}}$) and direct transmission ($\mathbf{D}_{\boldsymbol{\alpha\beta}}$) matrices are the identity matrix (**I**) and zero matrix (0), respectively, satisfying:$\{\mathbf{A}_{\boldsymbol{\alpha\beta}}, \mathbf{C}_{\boldsymbol{\alpha\beta}}\} \in \mathcal{M}_{4x4}$ and $\{\mathbf{B}_{\boldsymbol{\alpha\beta}}, \mathbf{D}_{\boldsymbol{\alpha\beta}}\} \in \mathcal{M}_{4x2}$.

To obtain the state-space representation in dq coordinates, the $\mathbf{K_p}$ matrix (defined in (14)) is applied to the model in αβ coordinates, resulting in (23). Here, the state, output, and input vectors in dq coordinates are: $\mathbf{q}_{\mathbf{dq}}(t) = [q_{1d}(t), q_{1q}(t), q_{2d}(t), q_{2q}(t)]^\mathrm{T}$, $\mathbf{y}_{\mathbf{dq}}(t) = \mathbf{q}_{\mathbf{dq}}(t)$, and $\mathbf{u}_{\mathbf{dq}}(t) = [u_{1d}(t), u_{1q}(t)]^\mathrm{T}$. These vectors can also be defined as $\{\mathbf{q}_{\mathbf{dq}}(t), \mathbf{y}_{\mathbf{dq}}(t)\} \in \{\mathbb{R}^4\}$ and $\mathbf{u}_{\mathbf{dq}}(t) \in \{\mathbb{R}^2\}$.

$$\begin{cases} \dfrac{\mathrm{d}\mathbf{q_{dq}}(t)}{\mathrm{d}t} = \mathbf{A_{dq}} \cdot \mathbf{q_{dq}}(t) + \mathbf{B_{dq}} \cdot \mathbf{u_{dq}}(t) \\ \mathbf{y_{dq}}(t) = \mathbf{C_{dq}} \cdot \mathbf{q_{dq}}(t) + \mathbf{D_{dq}} \cdot \mathbf{u_{dq}}(t) \end{cases} \tag{23}$$

In this model, $\mathbf{q_{dq}}(t)$, $\mathbf{y_{dq}}(t)$, and $\mathbf{u_{dq}}(t)$ represent the state, output, and input vectors in dq coordinates, respectively. Specifically, The matrices $\mathbf{A_{dq}}$ and $\mathbf{B_{dq}}$ are as described as follows:

$$\mathbf{A_{dq}} = \begin{bmatrix} 0 & \omega & 1 & 0 \\ -\omega & 0 & 0 & 1 \\ -\dfrac{k_{\mathrm{eq}_1}}{m_1} & 0 & -\dfrac{b_{\mathrm{eq}_1}}{m_1} & \omega \\ 0 & -\dfrac{k_{\mathrm{eq}_1}}{m_1} & -\omega & -\dfrac{b_{\mathrm{eq}_1}}{m_1} \end{bmatrix} \mathbf{B_{dq}} = \begin{bmatrix} 0 & 0 \\ 0 & 0 \\ \dfrac{1}{m_1} & 0 \\ 0 & \dfrac{1}{m_1} \end{bmatrix} \tag{24}$$

and the matrices $\mathbf{C_{dq}}$ and $\mathbf{D_{dq}}$ are identity and zero, respectively. Here, ω represents the angular frequency corresponding to the excitation force. Symbolically, the matrices can be defined as $\{\mathbf{A_{dq}}, \mathbf{C_{dq}}\} \in \mathcal{M}_{4x4}$ and $\{\mathbf{B_{dq}}, \mathbf{D_{dq}}\} \in \mathcal{M}_{4x1}$.

Extending this model, a linear electrical analogy can be derived to represent the mechanical system. The electrical model is shown in **Figure 3** and is developed for both the d and q channels. Each electrical network is configured using equivalent Thevenin circuits consisting of energy-storing elements (m_1 as inductor and $1/k_{\mathrm{eq}_1}$ as capacitor) and voltage sources controlled by charges ($q_{1j}(t)$ and $q_{2j}(t)$, where $j \in \{\mathrm{d}, \mathrm{q}\}$).

3.2 Analysis of a Mechanical-Vibrational-Dynamical System of Two-Degree-of-Freedom

This section examines the dynamic behavior of a 2-DoF vibrational mechanical system, illustrated in **Figure 2(b)**. The analysis follows the methodology applied to the 1-DoF system, extending it to derive the corresponding energy equations. The kinetic, potential, and dissipation energy expressions for the 2-DoF system are formulated as follows:

$$\begin{cases} KE(t) = \dfrac{1}{2} \cdot m_1 \cdot \dot{x}_1(t)^2 + \dfrac{1}{2} \cdot m_2 \cdot \dot{x}_2(t)^2 \\ PE(t) = \dfrac{1}{2} \cdot k_{\mathrm{eq}_1} \cdot x_1(t)^2 - k_2 \cdot x_1(t) \cdot x_2(t) + \dfrac{1}{2} \cdot k_{\mathrm{eq}_2} \cdot x_2(t)^2 \\ DE(t) = \dfrac{1}{2} \cdot b_{\mathrm{eq}_1} \cdot \dot{x}_1(t)^2 - b_2 \cdot \dot{x}_1(t) \cdot \dot{x}_2(t) + \dfrac{1}{2} \cdot b_{\mathrm{eq}_2} \cdot \dot{x}_2(t)^2 \end{cases} \tag{25}$$

where the equivalent damping and stiffness coefficients are defined as: $b_{\mathrm{eq1}} = b_1 + b_2$, $b_{\mathrm{eq2}} = b_2 + b_3$, $k_{\mathrm{eq1}} = k_1 + k_2$, and $k_{\mathrm{eq2}} = k_2 + k_3$. Applying (17) with $p_1(t) = x_1(t)$ and $p_2(t) = x_2(t)$, and performing algebraic manipulations, the 2-DoF system model is obtained in state-space representation. The state-space formulation enables a systematic representation of the vibrational system. The corresponding state-space equations are structured as follows in (18). For the sake of simplicity, the matrices **C** and **D** are the identities and zero matrices, the vector and matrix model of a vibrating system in mechanical coordinates in state-space representation follows the same, respectively. Mathematically, $\{\mathbf{A}, \mathbf{C}\} \in \mathcal{M}_{4x4}$ and $\{\mathbf{B}, \mathbf{D}\} \in \mathcal{M}_{4x1}$ where **A**, **B**, **C**, and **D** are the state matrix, input matrix, output matrix, and direct transmission matrix, respectively. The state vector components are defined as: $\mathbf{q}(t) = [q_1(t), q_2(t), q_3(t), q_4(t)]^{\mathrm{T}}$, the output vector $\mathbf{y}(t) = \mathbf{q}(t)$, and the scalar input $u(t) = f_1(t)$. Moreover, $q_1(t) = x_1(t)$, $q_2(t) = \mathrm{d}x_1(t)/\mathrm{d}t$, $q_3(t) = x_2(t)$, and $q_4(t) = \mathrm{d}x_2(t)/\mathrm{d}t$. Symbolically, $\{\mathbf{q}(t), \mathbf{y}(t)\} \in \{\mathbb{R}^4\}$.

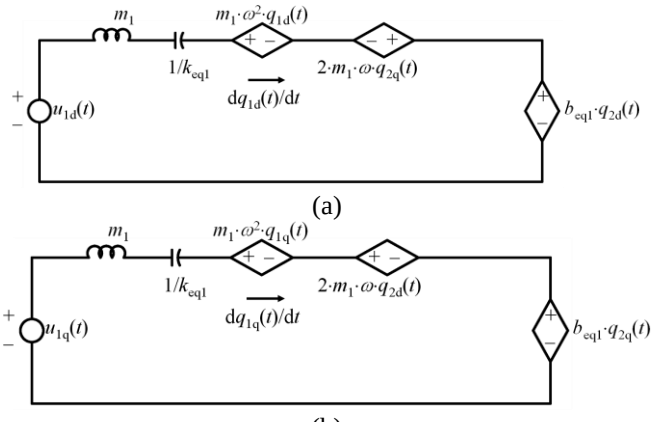

Figure 3. Electrical analogy of the proposed 1-DoF mechanical system in dq coordinates. The two channels d and q are shown. (a) Channel d. (b) Channel q

The state-space matrices governing the dynamics of the 2-DoF system are expressed as:

$$\mathbf{A} = \begin{bmatrix} 0 & 1 & 0 & 0 \\ -\frac{k_{eq_1}}{m_1} & -\frac{b_{eq_1}}{m_1} & \frac{k_2}{m_1} & \frac{b_2}{m_1} \\ 0 & 0 & 0 & 1 \\ \frac{k_2}{m_2} & \frac{b_2}{m_2} & -\frac{k_{eq_2}}{m_2} & -\frac{b_{eq_2}}{m_2} \end{bmatrix} \mathbf{B} = \begin{bmatrix} 0 \\ 0 \\ 0 \\ \frac{1}{m_2} \end{bmatrix} \tag{26}$$

The model (18) is then converted into αβ coordinates using the procedure developed previously in the 1-DoF system analysis. The equivalences defined as follows:

$$\begin{cases} q_{1\alpha}(t) = q_1(t), & q_{1\beta}(t) = q_1\left(t - \frac{\pi}{2}\right) \\ q_{2\alpha}(t) = q_2(t), & q_{2\beta}(t) = q_2\left(t - \frac{\pi}{2}\right) \\ q_{3\alpha}(t) = q_3(t), & q_{3\beta}(t) = q_3\left(t - \frac{\pi}{2}\right) \\ q_{4\alpha}(t) = q_4(t), & q_{4\beta}(t) = q_4\left(t - \frac{\pi}{2}\right) \\ u_\alpha(t) = u(t), & u_\beta(t) = u\left(t - \frac{\pi}{2}\right) \end{cases} \tag{27}$$

The 2-DoF vibrational mechanical system in αβ coordinates is formulated in state-space representation as described in (21). Consistent with the structural formulation of the mechanical coordinate model in (18), the state-space representation in αβ coordinates maintain the same fundamental structure, making it applicable to a generalized *n*-DoF system.

The system's vectors are expressed as follows: the state vector is defined as $\mathbf{q}_{\alpha\beta}(t) = [q_{1\alpha}(t), q_{1\beta}(t), q_{2\alpha}(t), q_{2\beta}(t), q_{3\alpha}(t), q_{3\beta}(t), q_{4\alpha}(t), q_{4\beta}(t)]^{\mathrm{T}}$, $\mathbf{y}_{\alpha\beta}(t) = \mathbf{q}_{\alpha\beta}(t)$, and $\mathbf{u}_{\alpha\beta}(t) = [u_{1\alpha}(t), u_{1\beta}(t)]^{\mathrm{T}}$, where $\mathbf{q}_{\alpha\beta}(t)$, $\mathbf{y}_{\alpha\beta}(t)$, and $\mathbf{u}_{\alpha\beta}(t)$ are the state, output, and input vectors, respectively. Symbolically, $\{\mathbf{q}_{\alpha\beta}(t), \mathbf{y}_{\alpha\beta}(t)\} \in \{\mathbb{R}^8\}$ and $\mathbf{u}_{\alpha\beta}(t) \in \{\mathbb{R}^2\}$, ensuring that the system adheres to an eight-dimensional state-space framework.

Furthermore, the state and input matrices associated with the αβ model are represented by $\mathbf{A}_{\alpha\beta}$ and $\mathbf{B}_{\alpha\beta}$, respectively, defined as follows:

$$\mathbf{A}_{\alpha\beta} = \begin{bmatrix} 0 & 0 & 1 & 0 & 0 & 0 & 0 & 0 \\ 0 & 0 & 0 & 1 & 0 & 0 & 0 & 0 \\ -\frac{k_{eq_1}}{m_1} & 0 & -\frac{b_{eq_1}}{m_1} & 0 & \frac{k_2}{m_1} & \frac{k_2}{m_1} & \frac{b_2}{m_1} & 0 \\ 0 & -\frac{k_{eq_1}}{m_1} & 0 & -\frac{b_{eq_1}}{m_1} & 0 & 0 & 0 & \frac{b_2}{m_1} \\ 0 & 0 & 0 & 0 & 0 & 0 & 1 & 0 \\ 0 & 0 & 0 & 0 & 0 & 0 & 0 & 1 \\ \frac{k_2}{m_2} & 0 & \frac{b_2}{m_2} & 0 & -\frac{k_{eq_2}}{m_2} & 0 & -\frac{b_{eq_2}}{m_2} & 0 \\ 0 & \frac{k_2}{m_2} & 0 & \frac{b_2}{m_2} & 0 & -\frac{k_{eq_2}}{m_2} & 0 & -\frac{b_{eq_2}}{m_2} \end{bmatrix}$$

$$\mathbf{B}_{\alpha\beta} = \begin{bmatrix} 0 & 0 & 1 & 0 & 0 & 0 & 0 & 0 \\ 0 & 0 & 0 & 1 & 0 & 0 & 0 & 0 \\ -\frac{k_{eq_1}}{m_1} & 0 & -\frac{b_{eq_1}}{m_1} & 0 & \frac{k_2}{m_1} & \frac{k_2}{m_1} & \frac{b_2}{m_1} & 0 \\ 0 & -\frac{k_{eq_1}}{m_1} & 0 & -\frac{b_{eq_1}}{m_1} & 0 & 0 & 0 & \frac{b_2}{m_1} \\ 0 & 0 & 0 & 0 & 0 & 0 & 1 & 0 \\ 0 & 0 & 0 & 0 & 0 & 0 & 0 & 1 \\ \frac{k_2}{m_2} & 0 & \frac{b_2}{m_2} & 0 & -\frac{k_{eq_2}}{m_2} & 0 & -\frac{b_{eq_2}}{m_2} & 0 \\ 0 & \frac{k_2}{m_2} & 0 & \frac{b_2}{m_2} & 0 & -\frac{k_{eq_2}}{m_2} & 0 & -\frac{b_{eq_2}}{m_2} \end{bmatrix} \tag{28}$$

These matrices are defined as in Eq (28), maintaining consistency with the transformation applied to obtain the αβ coordinate formulation from its original mechanical representation. In addition, $\mathbf{C}_{\alpha\beta}$ and $\mathbf{D}_{\alpha\beta}$ are the output and direct transmission matrices representing the identity and zero matrices, respectively. Symbolically, $\{\mathbf{A}_{\alpha\beta}, \mathbf{C}_{\alpha\beta}\} \in \mathscr{M}_{8x8}$ and $\{\mathbf{B}_{\alpha\beta}, \mathbf{D}_{\alpha\beta}\} \in \mathscr{M}_{8x2}$.

As the final step in the transformation process, the αβ coordinate model is converted into the dq reference frame. This transformation follows the same methodology as the 1-DoF system analysis, where the $\mathbf{K}_\mathbf{p}$ matrix is applied to (21) to derive the state-space representation of the 2-DoF vibrational mechanical system in dq coordinates, as outlined in (23). Notably, the vector-matrix representation for an *n*-DoF mechanical system retains the same structural format as presented in (23), ensuring scalability and general applicability.

The state-space vectors for the dq coordinate system are structured as follows: the state vector is $\mathbf{q}_{\mathbf{dq}}(t) = [q_{1d}(t), q_{1q}(t), q_{2d}(t), q_{2q}(t), q_{3d}(t), q_{3q}(t), q_{4d}(t), q_{4q}(t)]^T$, the output vector is $\mathbf{y}_{\mathbf{dq}}(t) = \mathbf{q}_{\mathbf{dq}}(t)$, and the input vector is $\mathbf{u}_{\mathbf{dq}}(t) = [u_{1d}(t), u_{1q}(t)]^T$. These vectors are mathematically defined within the spaces $\{\mathbf{q}_{\mathbf{dq}}(t), \mathbf{y}_{\mathbf{dq}}(t)\} \in \{\mathbb{R}^8\}$ and $\mathbf{u}_{\mathbf{dq}}(t) \in \{\mathbb{R}^2\}$, preserving the system's dynamic characteristics under the transformation.

Following the approach used for the 1-DoF system, an electrical analogy model is developed for the 2-DoF system, as illustrated in **Figure 4**. These equivalent circuits leverage Thévenin voltage representations, where each channel—d and q—is represented separately. As depicted in **Figure 4(a)** and **(b)**, the 2-DoF system introduces an increased number of state variables per channel, effectively doubling those present in the 1-DoF case, thereby highlighting the expanded complexity of the system's vibrational dynamics in the dq domain.

3.3 Analysis of a Mechanical-Vibrational-Dynamical System of Three-Degree-of-Freedom

This section examines the dynamics of a 3-DoF vibrational mechanical system, as illustrated in **Figure 2(c)**. The energy equations governing the system, which encompass kinetic, potential, and dissipation energy components, are expressed as follows:

$$\begin{cases} KE(t) = \frac{1}{2}\cdot m_1 \cdot \dot{x}_1(t)^2 + \frac{1}{2}\cdot m_2 \cdot \dot{x}_2(t)^2 + \frac{1}{2}\cdot m_3 \cdot \dot{x}_3(t)^2 \\ PE(t) = \frac{1}{2}\cdot k_{\mathrm{eq}_1} \cdot x_1(t)^2 + \frac{1}{2}\cdot k_{\mathrm{eq}_2} \cdot x_2(t)^2 + \frac{1}{2}\cdot k_{\mathrm{eq}_3} \cdot x_3(t)^2 - k_2 \cdot x_1(t) \cdot x_2(t) - k_3 \cdot x_2(t) \cdot x_3(t) \\ DE(t) = \frac{1}{2}\cdot b_{\mathrm{eq}_1} \cdot \dot{x}_1(t)^2 + \frac{1}{2}\cdot b_{\mathrm{eq}_2} \cdot \dot{x}_2(t)^2 + \frac{1}{2}\cdot b_{\mathrm{eq}_3} \cdot \dot{x}_3(t)^2 - b_2 \cdot \dot{x}_1(t) \cdot \dot{x}_2(t) - b_3 \cdot \dot{x}_2(t) \cdot \dot{x}_3(t) \end{cases} \quad (29)$$

These equations follow the same formulation principles as those developed for the 1-DoF and 2-DoF systems. In this specific case, the system parameters are defined as $b_{eq1} = b_1 + b_2$, $b_{eq2} = b_2 + b_3$, $b_{eq3} = b_3 + b_4$, $k_{eq1} = k_1 + k_2$, $k_{eq2} = k_2 + k_3$, and $k_{eq3} = k_3 + k_4$.

By applying (17) to these energy expressions, the state-space dynamic model is derived and structured as shown in (18). The system is characterized by a state vector $\mathbf{q}(t) = [q_j(t)]^T$, where $j \in \{1, 2, 3, 4, 5, 6\}$, while the output vector follows $\mathbf{y}(t) = \mathbf{q}(t)$. The state variables are explicitly defined as follows: $q_1(t) = x_1(t)$, $q_2(t) = \mathrm{d}x_1(t)/\mathrm{d}t$, $q_3(t) = x_2(t)$, $q_4(t) = \mathrm{d}x_2(t)/\mathrm{d}t$, $q_5(t) = x_3(t)$, and $q_6(t) = \mathrm{d}x_3(t)/\mathrm{d}t$.

The scalar input affecting the system is denoted as $u(t) = f_1(t)$. Mathematically, the state-space representation of the system adheres to $\{\mathbf{q}(t), \mathbf{y}(t)\} \in \mathbb{R}^6$.

The state matrix (**A**) and input matrix (**B**) are structured as follows:

$$\mathbf{A} = \begin{bmatrix} 0 & 1 & 0 & 0 & 0 & 0 \\ -\frac{k_{\mathrm{eq}_1}}{m_1} & -\frac{b_{\mathrm{eq}_1}}{m_1} & \frac{k_2}{m_1} & \frac{b_2}{m_1} & 0 & 0 \\ 0 & 0 & 0 & 1 & 0 & 0 \\ \frac{k_2}{m_2} & \frac{b_2}{m_1} & -\frac{k_{\mathrm{eq}_2}}{m_2} & -\frac{b_{\mathrm{eq}_2}}{m_2} & \frac{k_{\mathrm{eq}_3}}{m_2} & \frac{b_3}{m_2} \\ 0 & 0 & 0 & 0 & 0 & 1 \\ 0 & 0 & \frac{k_{\mathrm{eq}_3}}{m_3} & \frac{b_3}{m_3} & -\frac{k_{\mathrm{eq}_3}}{m_3} & -\frac{b_{\mathrm{eq}_3}}{m_3} \end{bmatrix} \mathbf{B} = \begin{bmatrix} 0 \\ 0 \\ 0 \\ 0 \\ 0 \\ \frac{1}{m_3} \end{bmatrix} \quad (30)$$

Additionally, the output matrix (**C**) and the direct transmission matrix (**D**) are both identity and zero matrices, respectively. This representation can be expressed as $\{\mathbf{A}, \mathbf{C}\} \in \mathscr{M}_{6x6}$ and $\{\mathbf{B}, \mathbf{D}\} \in \mathscr{M}_{6x1}$.

To extend the analysis of the 3-DoF vibrational mechanical system, the transformation into αβ coordinates is performed following a methodology analogous to that used for the 1-DoF and 2-DoF systems. This transformation, as described in (21), introduces the notations $q_{i\alpha}(t) = q_i(t)$ and $q_{i\beta}(t) = q_i(t - \pi/2)$, while the external force components

transform as $u_\alpha(t) = u(t)$ and $u_\beta(t) = u(t - \pi/2)$. As a result, new state ($\mathbf{q_{\alpha\beta}}(t)$), input ($\mathbf{u_{\alpha\beta}}(t)$), and output ($\mathbf{y_{\alpha\beta}}(t)$) vectors are derived, where: $\mathbf{q_{\alpha\beta}}(t) = [q_{i\alpha}(t), q_{i\beta}(t)]^T$ for $i \in \{1, 2, 3, 4, 5, 6\}$, $\mathbf{y_{\alpha\beta}}(t) = \mathbf{q_{\alpha\beta}}(t)$, and $\mathbf{u_{\alpha\beta}}(t) = [u_\alpha(t), u_\beta(t)]^T$.

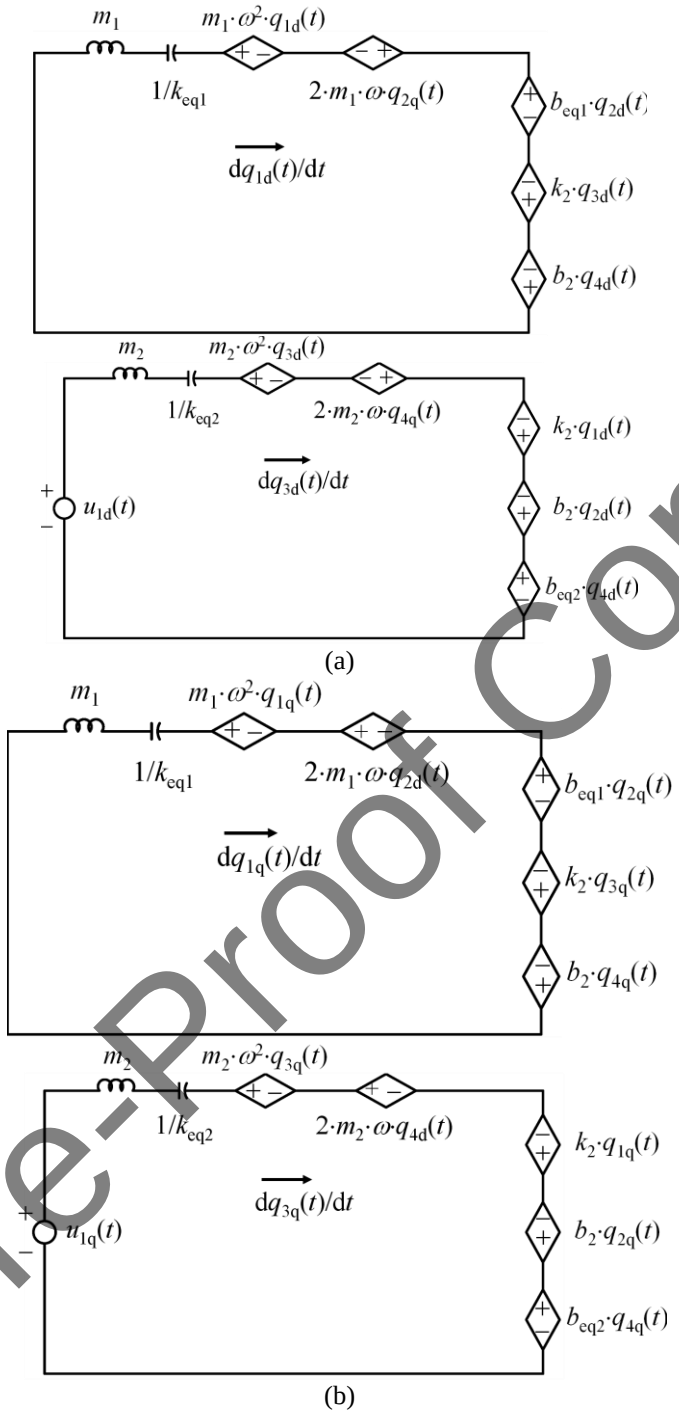

Figure 4. Electrical analogy of the proposed 2-DoF mechanical system in dq coordinates. The two channels d and q are shown. (a) Channel d. (b) Channel q

From a mathematical perspective, this transformation results in $\{\mathbf{q_{\alpha\beta}}(t), \mathbf{y_{\alpha\beta}}(t)\} \in \{\mathbb{R}^{12}\}$ and $\mathbf{u_{\alpha\beta}}(t) \in \{\mathbb{R}^2\}$. The state-space representation in αβ coordinates, derived from (21), is defined by the matrices:

$$\mathbf{A_{\alpha\beta}} = \begin{bmatrix} \mathbf{A_{\alpha\beta_{11}}} & \mathbf{A_{\alpha\beta_{12}}} \\ \mathbf{A_{\alpha\beta_{21}}} & \mathbf{A_{\alpha\beta_{22}}} \end{bmatrix};\ \mathbf{B_{\alpha\beta}} = \begin{bmatrix} \mathbf{B_{\alpha\beta_{11}}} \\ \mathbf{B_{\alpha\beta_{21}}} \end{bmatrix} \tag{31}$$

where $\mathbf{C_{\alpha\beta}}$ and $\mathbf{D_{\alpha\beta}}$ remain the identity and zero matrices, respectively.

The submatrices comprising $\mathbf{A_{\alpha\beta}}$ and $\mathbf{B_{\alpha\beta}}$ are explicitly given in (32) and (33), respectively. From a symbolic representation, $\{\mathbf{A_{\alpha\beta}}, \mathbf{C_{\alpha\beta}}\} \in \mathcal{M}_{12x12}$ and $\{\mathbf{B_{\alpha\beta}}, \mathbf{D_{\alpha\beta}}\} \in \mathcal{M}_{12x2}$.

To further develop the model, the $\mathbf{K_p}$ matrix is applied to the system in αβ coordinates, leading to the dq-domain state-space representation of the 3-DoF mechanical system, as described in (23). The state, output, and input vectors in dq coordinates are: $\mathbf{q_{dq}}(t) = [q_{id}(t), q_{iq}(t)]^T$ for $i \in \{1, 2, 3, 4, 5, 6\}$, $\mathbf{y_{dq}}(t) = \mathbf{q_{dq}}(t)$, and $u_{dq}(t) = [u_d(t), u_q(t)]^T$.

$$\mathbf{A}_{\alpha\beta_{11}} = \begin{bmatrix} 0 & 0 & 1 & 0 & 0 & 0 \\ 0 & 0 & 0 & 1 & 0 & 0 \\ -\frac{k_{eq_1}}{m_1} & 0 & -\frac{b_{eq_1}}{m_1} & 0 & \frac{k_2}{m_1} & 0 \\ 0 & -\frac{k_{eq_1}}{m_1} & 0 & -\frac{b_{eq_1}}{m_1} & 0 & \frac{k_2}{m_1} \\ 0 & 0 & 0 & 0 & 0 & 0 \\ 0 & 0 & 0 & 0 & 0 & 0 \end{bmatrix}; \mathbf{A}_{\alpha\beta_{12}} = \begin{bmatrix} 0 & 0 & 0 & 0 & 0 & 0 \\ 0 & 0 & 0 & 0 & 0 & 0 \\ \frac{b_2}{m_1} & 0 & 0 & 0 & 0 & 0 \\ 0 & \frac{b_2}{m_1} & 0 & 0 & 0 & 0 \\ 0 & 0 & 0 & 0 & 0 & 0 \\ 1 & 0 & 0 & 0 & 0 & 0 \end{bmatrix};$$

$$\mathbf{A}_{\alpha\beta_{21}} = \begin{bmatrix} \frac{k_2}{m_2} & 0 & \frac{b_2}{m_2} & 0 & -\frac{k_{eq_2}}{m_2} & 0 \\ 0 & \frac{k_2}{m_2} & 0 & \frac{b_2}{m_2} & 0 & -\frac{k_{eq_2}}{m_2} \\ 0 & 0 & 0 & 0 & 0 & 0 \\ 0 & 0 & 0 & 0 & 0 & 0 \\ 0 & 0 & 0 & 0 & \frac{k_3}{m_3} & 0 \\ 0 & 0 & 0 & 0 & 0 & \frac{k_3}{m_3} \end{bmatrix}; \tag{32}$$

$$\mathbf{A}_{\alpha\beta_{22}} = \begin{bmatrix} -\frac{b_{eq_2}}{m_2} & 0 & \frac{k_3}{m_2} & 0 & \frac{b_3}{m_2} & 0 \\ 0 & -\frac{b_{eq_2}}{m_2} & 0 & \frac{k_3}{m_2} & 0 & \frac{b_3}{m_2} \\ 0 & 0 & 0 & 0 & 1 & 0 \\ 0 & 0 & 0 & 0 & 0 & 1 \\ \frac{b_3}{m_3} & 0 & -\frac{k_{eq_3}}{m_3} & 0 & -\frac{b_{eq_3}}{m_3} & 0 \\ 0 & \frac{b_3}{m_3} & 0 & -\frac{k_{eq_3}}{m_3} & 0 & -\frac{b_{eq_3}}{m_3} \end{bmatrix}$$

$$\mathbf{B}_{\alpha\beta_{11}} = \mathbf{0}; \mathbf{B}_{\alpha\beta_{21}} = \begin{bmatrix} 0 & 0 \\ 0 & 0 \\ 0 & 0 \\ 0 & 0 \\ \frac{1}{m_3} & 0 \\ 0 & \frac{1}{m_3} \end{bmatrix} \tag{33}$$

This system is characterized mathematically as $\{\mathbf{q_{dq}}(t), \mathbf{y_{dq}}(t)\} \in \{\mathbb{R}^{12}\}$, with $\mathbf{u_{dq}}(t) \in \{\mathbb{R}^2\}$. The state-space formulation in dq coordinates follows:

$$\mathbf{A_{dq}} = \begin{bmatrix} \mathbf{A_{dq_{11}}} & \mathbf{A_{dq_{12}}} \\ \mathbf{A_{dq_{21}}} & \mathbf{A_{dq_{22}}} \end{bmatrix}; \mathbf{B_{dq}} = \begin{bmatrix} \mathbf{B_{dq_{11}}} \\ \mathbf{B_{dq_{21}}} \end{bmatrix} \tag{34}$$

where the output ($\mathbf{C_{dq}}$) and direct transmission ($\mathbf{D_{dq}}$) matrices remain identity and zero matrices, respectively.

The submatrices of $\mathbf{A_{dq}}$ and $\mathbf{B_{dq}}$ are structured as indicated in (35) and (36).

An electrical analogy for the 3-DoF mechanical system is established based on the Thévenin equivalent circuit approach, as defined in (23). The corresponding circuit model is illustrated in **Figure 5**, with separate d- and q-channel representations shown in **Figure 5(a)** and **(b)**.

One notable conclusion from this analysis is that all 1, 2-, and 3-DoF models retain their linear properties regardless of the applied transformation. This is due to the intrinsically linear nature of the mechanical system and the linear

transformations involved [36], [37]. Additionally, the dq models exhibit inter-variable coupling, which can be eliminated through nodal transformations, thereby reducing the system to uncoupled equations based on its eigenvalues [38]. Furthermore, the electrical analogy circuit models can be seamlessly implemented in simulation platforms, facilitating behavioral analysis and computational validation.

$$\mathbf{A_{dq_{11}}} = \begin{bmatrix} 0 & \omega & 1 & 0 & 0 & 0 \\ -\omega & 0 & 0 & 1 & 0 & 0 \\ -\frac{k_{eq_1}}{m_1} & 0 & -\frac{b_{eq_1}}{m_1} & \omega & \frac{k_2}{m_1} & 0 \\ 0 & -\frac{k_{eq_1}}{m_1} & -\omega & -\frac{b_{eq_1}}{m_1} & 0 & \frac{k_2}{m_1} \\ 0 & 0 & 0 & 0 & 0 & \omega \\ 0 & 0 & 0 & 0 & -\omega & 0 \end{bmatrix}; \mathbf{A_{dq_{12}}} = \begin{bmatrix} 0 & 0 & 0 & 0 & 0 & 0 \\ 0 & 0 & 0 & 0 & 0 & 0 \\ \frac{b_2}{m_1} & 0 & 0 & 0 & 0 & 0 \\ 0 & \frac{b_2}{m_1} & 0 & 0 & 0 & 0 \\ 1 & 0 & 0 & 0 & 0 & 0 \\ 0 & 1 & 0 & 0 & 0 & 0 \end{bmatrix}$$

$$\mathbf{A_{dq_{21}}} = \begin{bmatrix} \frac{k_2}{m_2} & 0 & \frac{b_2}{m_2} & 0 & -\frac{k_{eq_2}}{m_2} & 0 \\ 0 & \frac{k_2}{m_2} & 0 & \frac{b_2}{m_2} & 0 & -\frac{k_{eq_2}}{m_2} \\ 0 & 0 & 0 & 0 & 0 & 0 \\ 0 & 0 & 0 & 0 & 0 & 0 \\ 0 & 0 & 0 & 0 & \frac{k_3}{m_3} & 0 \\ 0 & 0 & 0 & 0 & 0 & \frac{k_3}{m_3} \end{bmatrix}; \tag{35}$$

$$\mathbf{A_{dq_{22}}} = \begin{bmatrix} -\frac{b_{eq_2}}{m_2} & \omega & \frac{k_3}{m_2} & 0 & \frac{b_3}{m_2} & 0 \\ -\omega & -\frac{b_{eq_2}}{m_2} & 0 & \frac{k_3}{m_2} & 0 & \frac{b_3}{m_2} \\ 0 & 0 & 0 & \omega & 1 & 0 \\ 0 & 0 & -\omega & 0 & 0 & 1 \\ \frac{b_3}{m_3} & 0 & -\frac{k_{eq_3}}{m_3} & 0 & -\frac{b_{eq_3}}{m_3} & \omega \\ 0 & \frac{b_3}{m_3} & 0 & -\frac{k_{eq_3}}{m_3} & -\omega & -\frac{b_{eq_3}}{m_3} \end{bmatrix}$$

$$\mathbf{B_{\alpha\beta_{11}}} = \mathbf{0}\ ;\ \mathbf{B_{\alpha\beta_{21}}} = \begin{bmatrix} 0 & 0 \\ 0 & 0 \\ 0 & 0 \\ 0 & 0 \\ \frac{1}{m_3} & 0 \\ 0 & \frac{1}{m_3} \end{bmatrix} \tag{36}$$

4.0 ANALYSIS OF ENERGY EQUATIONS: MECHANICAL ENERGY CURVES AND DQ ENERGY SURFACES IN 1-, 2-, AND 3-DOF SYSTEMS

The investigation of energy equations within both mechanical and dq coordinate systems for vibrational mechanical systems with 1-, 2-, and 3-DoF offers significant insights into system dynamics. This study provides a quantitative assessment of energy losses, identifies resonance effects, supports control and optimization strategies, and facilitates comparative evaluations across different coordinate systems. Additionally, this analysis serves as an educational tool and extends its applicability to interdisciplinary domains, contributing to the broader advancement of engineering and applied mechanics [39], [40].

In this work, the energy equations in mechanical coordinates have been previously derived for:

- The 1-DoF system, given in (16),
- The 2-DoF system, detailed in (25), and
- The 3-DoF system, formulated in (29).

Building upon these formulations, the expressions for kinetic, potential, and dissipation energy in dq coordinates are now derived.

To streamline the transformation process, the energy equations in mechanical coordinates for the 1-DoF system (16) are restated as follows:

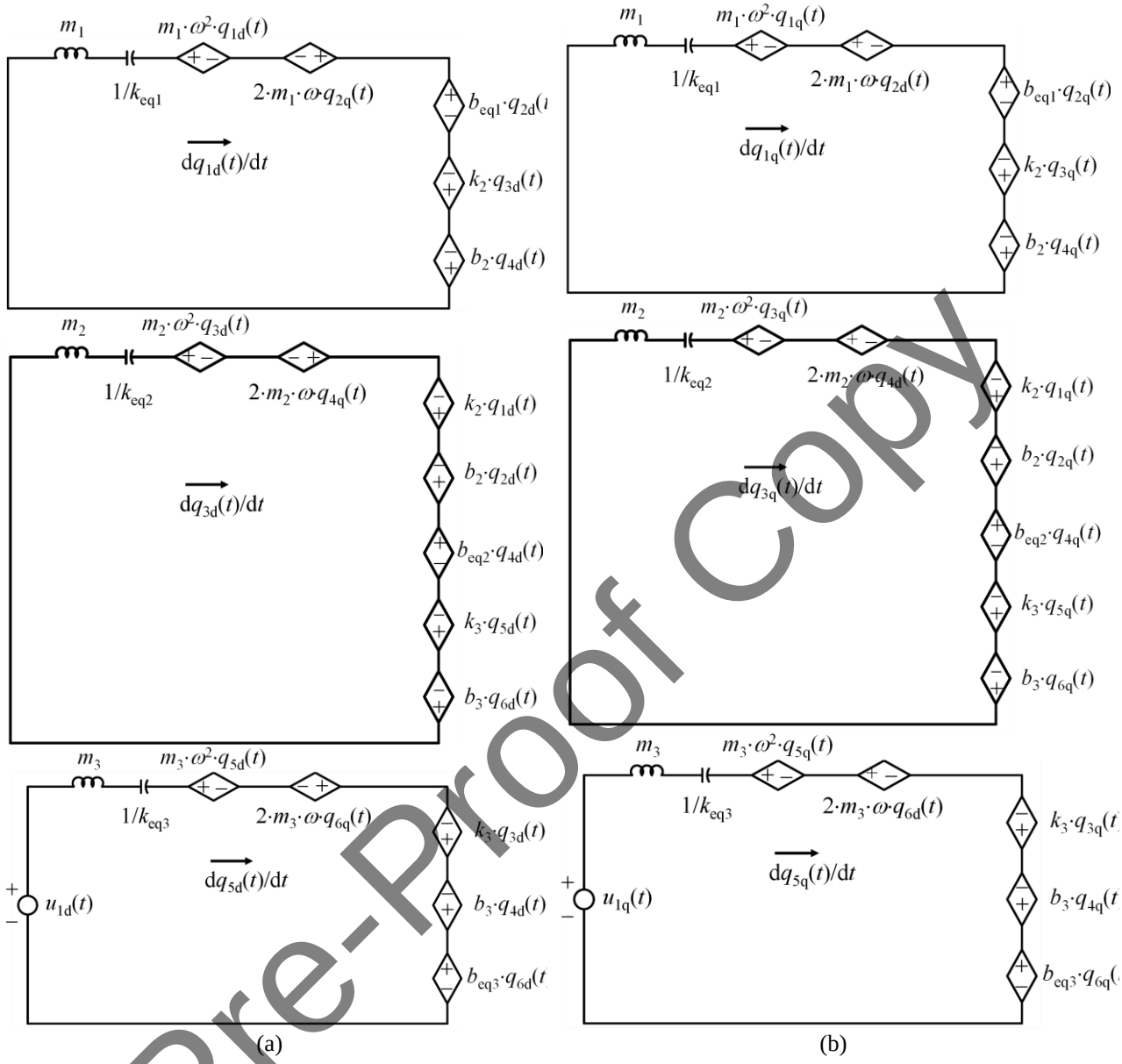

Figure 5. Electrical analogy of the proposed 3-DoF mechanical system in dq coordinates. The two channels d and q are shown. (a) Channel d. (b) Channel q

$$\begin{cases} KE(t) = \frac{1}{2} \cdot m_1 \cdot \dot{x}_1(t)^2 \\ PE(t) = \frac{1}{2} \cdot k_{\mathrm{eq}_1} \cdot x_1(t)^2 \\ DE(t) = \frac{1}{2} \cdot b_{\mathrm{eq}_1} \cdot \dot{x}_1(t)^2 \end{cases} \tag{37}$$

The kinetic energy expression is initially converted into αβ coordinates using the transformation approach developed in earlier sections. The corresponding expression is:

$$KE_{\alpha\beta}(t) = \frac{1}{2} \cdot m_1 \cdot [\dot{x}_{1\alpha}(t) \quad \dot{x}_{1\beta}(t)] \cdot \begin{bmatrix} \dot{x}_{1\alpha}(t) \\ \dot{x}_{1\beta}(t) \end{bmatrix}^{\mathrm{T}} \tag{38}$$

Applying the $\mathbf{K_p}$ transformation matrix to (38) results in the kinetic energy expression in dq coordinates, as given in (39).

Applying the same transformation approach to the potential energy and dissipation energy expressions, their dq-coordinate equivalents are obtained in (40).

Some key takeaways and implications can be:

$$\begin{cases} KE_{\mathrm{dq}}(t) = \dfrac{1}{2}\cdot m_1 \cdot \left(\mathbf{K_p}\cdot\begin{bmatrix}\dot{x}_{1\mathrm{d}}(t)\\ \dot{x}_{1\mathrm{q}}(t)\end{bmatrix}\right)^{\mathrm{T}}\cdot \mathbf{K_p}\cdot\begin{bmatrix}\dot{x}_{1\mathrm{d}}(t)\\ \dot{x}_{1\mathrm{q}}(t)\end{bmatrix} \\ KE_{\mathrm{dq}}(t) = \dfrac{1}{2}\cdot m_1 \cdot [\dot{x}_{1\mathrm{d}}(t) \quad \dot{x}_{1\mathrm{q}}(t)]\cdot \mathbf{K_p}^{\mathrm{T}}\cdot \mathbf{K_p}\cdot\begin{bmatrix}\dot{x}_{1\mathrm{d}}(t)\\ \dot{x}_{1\mathrm{q}}(t)\end{bmatrix} \\ KE_{\mathrm{dq}}(t) = \dfrac{1}{2}\cdot m_1 \cdot \left(\dot{x}_{1\mathrm{d}}(t)^2 + \dot{x}_{1\mathrm{q}}(t)^2\right) \end{cases} \tag{39}$$

$$\begin{cases} PE_{\mathrm{dq}}(t) = \dfrac{1}{2}\cdot k_{\mathrm{eq}_1} \cdot \left(x_{1\mathrm{d}}(t)^2 + x_{1\mathrm{q}}(t)^2\right) \\ DE_{\mathrm{dq}}(t) = \dfrac{1}{2}\cdot b_{\mathrm{eq}_1} \cdot \left(\dot{x}_{1\mathrm{d}}(t)^2 + \dot{x}_{1\mathrm{q}}(t)^2\right) \end{cases} \tag{40}$$

- Energy invariance across transformations: The total energy remains invariant under the dq transformation, confirming the preservation of physical properties in the new coordinate system.
- Simplification of control design: The separation of d and q components in the transformed equations enables easier implementation of control techniques, particularly for applications involving resonance suppression and energy regulation.
- Comparative analysis with mechanical coordinates: The transformation highlights differences in energy distribution and provides insights into damping effects, energy losses, and system response in both mechanical and dq domains.

By leveraging these energy equations in dq coordinates, this study advances the analytical methods used in vibration analysis and contributes to the enhancement of dynamic system modeling.

4.1 Derivation of the expressions for the kinetic, potential, and dissipation energies involved in the 2-DoF system

Applying the same procedure developed in the case of 1-DoF, the expressions of *KE*(*t*), *PE*(*t*), and *DE*(*t*) in dq coordinates related to the case of the 2-DoF system are obtained and defined as follows

$$\begin{cases} KE_{\mathrm{dq}}(t) = \dfrac{1}{2}\cdot m_1 \cdot \left(\dot{x}_{1\mathrm{d}}(t)^2 + \dot{x}_{1\mathrm{q}}(t)^2\right) + \dfrac{1}{2}\cdot m_2 \cdot \left(\dot{x}_{2\mathrm{d}}(t)^2 + \dot{x}_{2\mathrm{q}}(t)^2\right) \\ PE_{\mathrm{dq}}(t) = \dfrac{1}{2}\cdot k_{\mathrm{eq}_1} \cdot \left(x_{1\mathrm{d}}(t)^2 + x_{1\mathrm{q}}(t)^2\right) - k_2 \cdot \left(x_{1\mathrm{d}}(t)\cdot x_{2\mathrm{d}}(t) + x_{1\mathrm{q}}(t)\cdot x_{2\mathrm{q}}(t)\right) + \\ \qquad + \dfrac{1}{2}\cdot k_{\mathrm{eq}_2} \cdot \left(x_{2\mathrm{d}}(t)^2 + x_{2\mathrm{q}}(t)^2\right) \\ DE_{\mathrm{dq}}(t) = \dfrac{1}{2}\cdot b_{\mathrm{eq}_1} \cdot \left(\dot{x}_{1\mathrm{d}}(t)^2 + \dot{x}_{1\mathrm{q}}(t)^2\right) - b_2 \cdot \left(\dot{x}_{1\mathrm{d}}(t)\cdot \dot{x}_{2\mathrm{d}}(t) + \dot{x}_{1\mathrm{q}}(t)\cdot \dot{x}_{2\mathrm{q}}(t)\right) + \\ \qquad + \dfrac{1}{2}\cdot b_{\mathrm{eq}_2} \cdot \left(\dot{x}_{2\mathrm{d}}(t)^2 + \dot{x}_{2\mathrm{q}}(t)^2\right) \end{cases} \tag{41}$$

4.2 Derivation of the expressions for the kinetic, potential, and dissipation energies involved in the 3-DoF system

Following the same transformation methodology applied to the 1-DoF system, the kinetic energy (*KE*(*t*)), potential energy (*PE*(*t*)), and dissipation energy (*DE*(*t*)) equations are now derived for the 3-DoF vibrational mechanical system in dq coordinates. These energy expressions are obtained through the direct application of the dq transformation to the original equations formulated in mechanical coordinates, ensuring consistency with the previous analytical approach.

By systematically extending the transformation process, the resulting energy equations in dq coordinates for the 3-DoF system are expressed as follows:

$$\begin{cases} KE_{\mathrm{dq}}(t) = \frac{1}{2}\cdot m_1\cdot\left(\dot{x}_{1\mathrm{d}}(t)^2+\dot{x}_{1\mathrm{q}}(t)^2\right)+\frac{1}{2}\cdot m_2\cdot\left(\dot{x}_{2\mathrm{d}}(t)^2+\dot{x}_{2\mathrm{q}}(t)^2\right)+\frac{1}{2}\cdot m_3\cdot\left(\dot{x}_{3\mathrm{d}}(t)^2+\dot{x}_{3\mathrm{q}}(t)^2\right) \\ PE_{\mathrm{dq}}(t) = \frac{1}{2}\cdot k_{\mathrm{eq}_1}\cdot\left(x_{1\mathrm{d}}(t)^2+x_{1\mathrm{q}}(t)^2\right)+\frac{1}{2}\cdot k_{\mathrm{eq}_2}\cdot\left(x_{2\mathrm{d}}(t)^2+x_{2\mathrm{q}}(t)^2\right)+\frac{1}{2}\cdot k_{\mathrm{eq}_3}\cdot\left(x_{3\mathrm{d}}(t)^2+x_{3\mathrm{q}}(t)^2\right) \\ \quad -k_2\cdot\left(x_{1\mathrm{d}}(t)\cdot x_{2\mathrm{d}}(t)+x_{1\mathrm{q}}(t)\cdot x_{2\mathrm{q}}(t)\right)-k_3\cdot\left(x_{2\mathrm{d}}(t)\cdot x_{3\mathrm{d}}(t)+x_{2\mathrm{q}}(t)\cdot x_{3\mathrm{q}}(t)\right)+ \\ \quad +\frac{1}{2}\cdot k_{\mathrm{eq}_2}\cdot\left(x_{2\mathrm{d}}(t)^2+x_{2\mathrm{q}}(t)^2\right) \\ DE_{\mathrm{dq}}(t) = \frac{1}{2}\cdot b_{\mathrm{eq}_1}\cdot\left(\dot{x}_{1\mathrm{d}}(t)^2+\dot{x}_{1\mathrm{q}}(t)^2\right)+\frac{1}{2}\cdot b_{\mathrm{eq}_2}\cdot\left(\dot{x}_{2\mathrm{d}}(t)^2+\dot{x}_{2\mathrm{q}}(t)^2\right)++\frac{1}{2}\cdot b_{\mathrm{eq}_3}\cdot\left(\dot{x}_{2\mathrm{d}}(t)^2+\dot{x}_{2\mathrm{q}}(t)^2\right) \\ \quad -b_2\cdot\left(\dot{x}_{1\mathrm{d}}(t)\cdot\dot{x}_{2\mathrm{d}}(t)+\dot{x}_{1\mathrm{q}}(t)\cdot\dot{x}_{2\mathrm{q}}(t)\right)-b_3\cdot\left(\dot{x}_{2\mathrm{d}}(t)\cdot\dot{x}_{3\mathrm{d}}(t)+\dot{x}_{2\mathrm{q}}(t)\cdot\dot{x}_{3\mathrm{q}}(t)\right) \end{cases} \tag{42}$$

These transformed equations provide a comprehensive representation of the system's energy dynamics in the dq reference frame, facilitating deeper insights into energy distribution, dissipation mechanisms, and resonance behavior within the 3-DoF vibrational model.

5.0 SOLUTION OF THE SYSTEM IN MECHANICAL AND dq COORDINATES

To achieve a comprehensive understanding of the state variable dynamics within the studied vibrational mechanical systems, it is essential to derive their mathematical expressions by solving the governing dynamic models based on the equations of motion. This process enables a systematic investigation of the variables in both mechanical coordinates and the dq reference frame, providing a rigorous foundation for analytical comparisons.

The primary objective of this section is to:

- Establish the mathematical structures for each state variable.
- Compare these analytical solutions with simulation results to validate model accuracy.
- Present a formal representation of the mathematical formulations governing the system behavior.

By systematically deriving these expressions, the analysis not only facilitates a direct evaluation of system dynamics but also strengthens the interpretation of transformations between the mechanical and dq domains, ultimately enhancing the precision of the proposed vibrational system models.

5.1 Solution for 1-DoF in mechanical coordinates

The equation of motion (EoM) for the 1-DoF vibrational mechanical system is given in (17) and is rewritten explicitly as:

$$m_1\cdot\ddot{x}_1(t)+b_{\mathrm{eq1}}\cdot\dot{x}_1(t)+k_{\mathrm{eq1}}\cdot x_1(t)=F\cdot\sin(\omega\cdot t) \tag{43}$$

where $x_1(t)$ represents the displacement of the system, and all system parameters are previously defined in Section 3.0.

To determine the general solution for $x_1(t)$, the solving (43) by obtaining both the homogeneous (complementary) solution and the particular solution, which are then summed to derive the complete response of the system [41], [42].

The homogeneous component is derived from the unforced version of (43):

$$m_1\cdot\ddot{x}_{1\mathrm{c}}(t)+b_{\mathrm{eq1}}\cdot\dot{x}_{1\mathrm{c}}(t)+k_{\mathrm{eq1}}\cdot x_{1\mathrm{c}}(t)=0 \tag{44}$$

where $x_{1c}(t)$ represents the complementary part of $x_1(t)$.

By assuming a trial solution of the form: $x_{1c}(t) = \mathrm{e}^{(D\cdot t)}$ and substituting it into (44), the characteristic equation is obtained:

$$m_1\cdot D^2+b_{\mathrm{eq1}}\cdot D+k_{\mathrm{eq1}}=0 \tag{45}$$

Solving for D, the roots of the characteristic equation are:

$$D_{1,2}=-\alpha\pm\mathrm{j}\cdot\zeta,\ \text{where::}\ x_{1\mathrm{c}}(t)=C_1\cdot\mathrm{e}^{-(\alpha-\mathrm{j}\cdot\zeta)\cdot t}+C_2\cdot\mathrm{e}^{-(\alpha+\mathrm{j}\cdot\zeta)\cdot t} \tag{46}$$

where C_1 and C_2 are integration constants determined by initial conditions [41], [42].

Using Euler's equation [43] and trigonometric identities, the above expression can be rewritten as:

$$x_{1c}(t) = e^{-\alpha \cdot t} \cdot (X_1 \cdot \cos(\zeta \cdot t) + X_2 \cdot \sin(\zeta \cdot t)) \tag{47}$$

where $X_1 = C_1 + C_2$ and $X_2 = j \cdot (C_1 - C_2)$.

For the forced response, a particular solution of the following form is assumed, using the indeterminate coefficients method [41], i.e., $x_{1p}(t) = A \cdot \cos(\omega \cdot t) + B \cdot \sin(\omega \cdot t)$. Differentiating: $\dot{x}_{1p}(t) = -A \cdot \omega \cdot \sin(\omega \cdot t) + B \cdot \omega \cdot \cos(\omega \cdot t)$ and $\ddot{x}_{1p}(t) = -A \cdot \omega^2 \cdot \sin(\omega \cdot t) - B \cdot \omega^2 \cdot \cos(\omega \cdot t)$. In addition, A and B are coefficients to be determined. Substituting these into (43) and equating the coefficients of $\sin(\omega \cdot t)$ and $\cos(\omega \cdot t)$, the following system is obtained:

$$\begin{bmatrix} k_{eq_1} - \omega^2 \cdot m_1 & \omega \cdot b_{eq_1} \\ -\omega \cdot b_{eq_1} & k_{eq_1} - \omega^2 \cdot m_1 \end{bmatrix} \cdot \begin{bmatrix} A \\ B \end{bmatrix} = \begin{bmatrix} 0 \\ F \end{bmatrix} \tag{48}$$

Solving for A and B as follows in (49). Applying trigonometric transformations, the total solution for $x_1(t)$ is given by (50).

$$\begin{cases} A = -\dfrac{F \cdot \omega \cdot b_{eq_1}}{\left(k_{eq_1} - \omega^2 \cdot m_1\right) + \left(\omega \cdot b_{eq_1}\right)^2} \\ B = -\dfrac{F \cdot \left(k_{eq_1} - \omega^2 \cdot m_1\right)}{\left(k_{eq_1} - \omega^2 \cdot m_1\right) + \left(\omega \cdot b_{eq_1}\right)^2} \end{cases} \tag{49}$$

$$x_1(t) = x_{1c}(t) + x_{1p}(t) = e^{-\alpha \cdot t} \cdot X \cdot \sin(\zeta \cdot t + \rho) + T \cdot \sin(\omega \cdot t + \phi) \tag{50}$$

where $X = \text{sqrt}(X_1^2 + X_2^2)$, $\rho = \text{atan}(X_1/X_2)$, $T = \text{sqrt}(A^2 + B^2)$, and $\phi = \text{atan}(A/B)$.

In order to interpretate the solution, one can state the following:

- The first term represents the transient response due to initial conditions, which decays exponentially over time at a rate defined by α.
- The second term represents the steady-state response, which follows the external forcing function but is shifted in phase by ϕ.

This solution provides a rigorous mathematical foundation for understanding oscillatory behavior in the 1-DoF vibrational system under sinusoidal excitation.

5.2 Solution for 1-DoF in dq coordinates

The EoM for the 1-DoF vibrational mechanical system in dq coordinates is derived from (23). Using the variable transformation $q_{1d}(t) = q_{2q}(t) = q_{2d}(t) = q_{2q}(t) = q_{2q}(t) = e^{(D \cdot t)}$, and substituting into (23), the resulting system model in terms of D is expressed as:

$$\begin{bmatrix} D & -\omega & -1 & 0 \\ \omega & D & 0 & -1 \\ \dfrac{k_{eq_1}}{m_1} & 0 & D + \dfrac{b_{eq_1}}{m_1} & -\omega \\ 0 & \dfrac{k_{eq_1}}{m_1} & \omega & D + \dfrac{b_{eq_1}}{m_1} \end{bmatrix} \cdot \begin{bmatrix} q_{1_d}(t) \\ q_{1_q}(t) \\ q_{2_d}(t) \\ q_{2_q}(t) \end{bmatrix} = \begin{bmatrix} 0 \\ 0 \\ \dfrac{u_{1_d}(t)}{m_1} \\ \dfrac{u_{1_q}(t)}{m_1} \end{bmatrix} \tag{51}$$

where $u_{1d}(t)$ and $u_{1q}(t)$ correspond to the d and q components of the external force acting on the transformed system.

By solving the unforced equation, the determination of the complementary solution of the system is given by:

$$\begin{gathered} \left(m_1^2 \cdot D^4 + 2 \cdot b_{eq1} \cdot m_1 \cdot D^3 + \left(b_{eq1}^2 + 2 \cdot m_1 \cdot \omega^2 + 2 \cdot k_{eq1} \cdot m_1\right) \cdot D^2 + \right. \\ + \left(2 \cdot b_{eq1} \cdot m_1 \cdot \omega^2 + 2 \cdot b_{eq1} \cdot k_{eq1}\right) \cdot D + b_{eq1}^2 \cdot \omega^2 + k_{eq1}^2 - 2 \cdot k_{eq1} \cdot m_1 \cdot \omega^2 + \\ \left. + m_1^2 \cdot \omega^4\right) \cdot e^{D \cdot t} = 0 \end{gathered} \tag{52}$$

Solving for D, the characteristic roots are:

$$\begin{cases} D_1 = -\frac{1}{2}\cdot\left(\frac{b_{\mathrm{eq}_1}+\mathrm{j}\cdot\Gamma_1}{m_1}\right), & D_2 = -\frac{1}{2}\cdot\left(\frac{b_{\mathrm{eq}_1}+\mathrm{j}\cdot\Gamma_2}{m_1}\right) \\ D_3 = -\frac{1}{2}\cdot\left(\frac{b_{\mathrm{eq}_1}-\mathrm{j}\cdot\Gamma_1}{m_1}\right), & D_4 = -\frac{1}{2}\cdot\left(\frac{b_{\mathrm{eq}_1}-\mathrm{j}\cdot\Gamma_2}{m_1}\right) \end{cases} \tag{53}$$

where Γ_1 and Γ_2 are defined as:

$$\begin{cases} \Gamma_1 = 2\cdot\left(k_{\mathrm{eq}_1}\cdot m_1 + {m_1}^2\cdot\omega^2 - \left(\frac{1}{2}\cdot b_{\mathrm{eq}_1}\right)^2 + \mathrm{j}\cdot m_1\cdot\omega\cdot\sqrt{{b_{\mathrm{eq}_1}}^2 - 4\cdot k_{\mathrm{eq}_1}\cdot m_1}\right)^{\frac{1}{2}} \\ \Gamma_2 = 2\cdot\left(k_{\mathrm{eq}_1}\cdot m_1 + {m_1}^2\cdot\omega^2 - \left(\frac{1}{2}\cdot b_{\mathrm{eq}_1}\right)^2 - \mathrm{j}\cdot m_1\cdot\omega\cdot\sqrt{{b_{\mathrm{eq}_1}}^2 - 4\cdot k_{\mathrm{eq}_1}\cdot m_1}\right)^{\frac{1}{2}} \end{cases} \tag{54}$$

Using these roots, the complementary solution for $q_{ijc}(t)$ (where $i \in \{1,2\}$ and $j \in \{\mathrm{d}, \mathrm{q}\}$) is:

$$q_{ij_\mathrm{c}}(t) = C_1\cdot\mathrm{e}^{-D_1\cdot t} + C_2\cdot\mathrm{e}^{-D_2\cdot t} + C_3\cdot\mathrm{e}^{-D_3\cdot t} + C_4\cdot\mathrm{e}^{-D_4\cdot t} \tag{55}$$

Where C_n where $n \in \{1, 2, 3, 4\}$ are integration constants determined from initial conditions. Applying Euler's equation and trigonometric transformations, the complementary solution can be rewritten as:

$$q_{ij_\mathrm{c}}(t) = \mathrm{e}^{-\alpha_{\mathrm{dq}}\cdot t}\cdot\left(X_{1_{\mathrm{dq}}}\cdot\cos\left(\zeta_{1_{\mathrm{dq}}}\cdot t + \rho_{1_{\mathrm{dq}}}\right) + X_{2_{\mathrm{dq}}}\cdot\sin\left(\zeta_{2_{\mathrm{dq}}}\cdot t + \rho_{2_{\mathrm{dq}}}\right)\right) \tag{56}$$

The particular solution is obtained using the method for solving linear differential equations with constant coefficients [42].

Starting with:

$$q_{1_{\mathrm{dp}}}(t) = \prod_{i=1}^{4}\frac{1}{D+D_i}\cdot F\cdot b_{\mathrm{eq}_1}\cdot\omega \tag{57}$$

Applying the variable change:

$$v_1(t) = \frac{1}{D+D_4}\cdot F\cdot b_{\mathrm{eq}_1}\cdot\omega \Rightarrow \frac{\mathrm{d}v_1(t)}{\mathrm{d}t} + D_4\cdot v_1(t) = F\cdot b_{\mathrm{eq}_1}\cdot\omega \tag{58}$$

Solving this equation, the result is:

$$V_1 = -2\cdot\left(\frac{F\cdot b_{\mathrm{eq}_1}\cdot\omega\cdot m_1}{b_{\mathrm{eq}_1}-\mathrm{j}\cdot\Gamma_2}\right) \tag{59}$$

Repeating the variable transformation process for $V_2(t)$, $V_3(t)$, and $V_4(t)$, one obtains:

$$\begin{cases} V_2 = -4\cdot\left(\frac{F\cdot b_{\mathrm{eq}_1}\cdot\omega\cdot {m_1}^2}{\left(b_{\mathrm{eq}_1}-\mathrm{j}\cdot\Gamma_1\right)\cdot\left(b_{\mathrm{eq}_1}-\mathrm{j}\cdot\Gamma_2\right)}\right) \\ V_3 = -4\cdot\left(\frac{F\cdot b_{\mathrm{eq}_1}\cdot\omega\cdot {m_1}^3}{\left(b_{\mathrm{eq}_1}-\mathrm{j}\cdot\Gamma_1\right)\cdot\left({b_{\mathrm{eq}_1}}^2+{\Gamma_2}^2\right)}\right) \\ q_{1_{\mathrm{dp}}}(t) = V_4 = 16\cdot\left(\frac{F\cdot b_{\mathrm{eq}_1}\cdot\omega\cdot {m_1}^4}{\left({b_{\mathrm{eq}_1}}^2+{\Gamma_1}^2\right)\cdot\left({b_{\mathrm{eq}_1}}^2+{\Gamma_2}^2\right)}\right) \end{cases} \tag{60}$$

The final expression for $q_{1\mathrm{d}}(t)$ is:

$$\begin{aligned} q_{1_\mathrm{d}}(t) = q_{1_{\mathrm{d_c}}}(t) + q_{1_{\mathrm{d_p}}}(t) = \mathrm{e}^{-\alpha_{\mathrm{dq}}\cdot t}\cdot\left(X_{1_{\mathrm{dq}}}\cdot\cos\left(\zeta_{1_{\mathrm{dq}}}\cdot t + \rho_{1_{\mathrm{dq}}}\right) + X_{2_{\mathrm{dq}}}\cdot\sin\left(\zeta_{2_{\mathrm{dq}}}\cdot t + \rho_{2_{\mathrm{dq}}}\right)\right) + \\ +16\cdot\left(\frac{F\cdot b_{\mathrm{eq}_1}\cdot\omega\cdot {m_1}^4}{\left({b_{\mathrm{eq}_1}}^2+{\Gamma_1}^2\right)\cdot\left({b_{\mathrm{eq}_1}}^2+{\Gamma_2}^2\right)}\right) \end{aligned} \tag{61}$$

Using a similar process, we obtain the remaining state variables . $q_{1q}(t)$, $q_{2d}(t)$, and $q_{2q}(t)$, are derived and shown as follows:

$$q_{1_q}(t) = e^{-\alpha_{dq}\cdot t}\cdot\left(X_{1_{dq}}\cdot\cos\left(\zeta_{1_{dq}}\cdot t+\rho_{1_{dq}}\right)+X_{2_{dq}}\cdot\sin\left(\zeta_{2_{dq}}\cdot t+\rho_{2_{dq}}\right)\right)+ \\ +16\cdot\left(\frac{F\cdot\left(k_{eq_1}-m_1\cdot\omega^2\right)\cdot {m_1}^4}{\left({b_{eq_1}}^2+{\Gamma_1}^2\right)\cdot\left({b_{eq_1}}^2+{\Gamma_2}^2\right)}\right) \tag{62}$$

$$q_{2_d}(t) = e^{-\alpha_{dq}\cdot t}\cdot\left(X_{1_{dq}}\cdot\cos\left(\zeta_{1_{dq}}\cdot t+\rho_{1_{dq}}\right)+X_{2_{dq}}\cdot\sin\left(\zeta_{2_{dq}}\cdot t+\rho_{2_{dq}}\right)\right)+ \\ +16\cdot\left(\frac{F\cdot\omega\cdot\left(k_{eq_1}-m_1\cdot\omega^2\right)\cdot {m_1}^4}{\left({b_{eq_1}}^2+{\Gamma_1}^2\right)\cdot\left({b_{eq_1}}^2+{\Gamma_2}^2\right)}\right) \tag{63}$$

$$q_{2_q}(t) = e^{-\alpha_{dq}\cdot t}\cdot\left(X_{1_{dq}}\cdot\cos\left(\zeta_{1_{dq}}\cdot t+\rho_{1_{dq}}\right)+X_{2_{dq}}\cdot\sin\left(\zeta_{2_{dq}}\cdot t+\rho_{2_{dq}}\right)\right)+ \\ +16\cdot\left(\frac{F+\omega^2\cdot {m_1}^4\cdot b_{eq_1}}{\left({b_{eq_1}}^2+{\Gamma_1}^2\right)\cdot\left({b_{eq_1}}^2+{\Gamma_2}^2\right)}\right) \tag{64}$$

5.3 Solution for 2-DoF in mechanical coordinates

The EoM for the 2-DoF vibrational mechanical system in mechanical coordinates is characterized by 17 and (25). However, for practical purposes, the EoMs are rewritten as shown as follows:

$$\begin{cases} m_1\cdot\ddot{x}_1(t)+b_{eq_1}\cdot\dot{x}_1(t)+k_{eq_1}\cdot x_1(t)-b_2\cdot\dot{x}_2(t)-k_2\cdot x_2(t)=0 \\ m_2\cdot\ddot{x}_2(t)+b_{eq_2}\cdot\dot{x}_2(t)+k_{eq_2}\cdot x_2(t)-b_2\cdot\dot{x}_1(t)-k_2\cdot x_1(t)=F\cdot\sin(\omega\cdot t) \end{cases} \tag{65}$$

Using the same solution method applied to the 1-DoF system (involving the complementary and particular solutions), the solutions for $x_1(t)$ and $x_2(t)$ are derived as follows:

$$\begin{cases} x_1(t)=e^{-\alpha_1\cdot t}\cdot X_1\cdot\sin(\zeta_1\cdot t+\rho_1)+e^{-\alpha_2\cdot t}\cdot X_2\cdot\sin(\zeta_2\cdot t+\rho_2)+T_1\cdot\sin(\omega\cdot t+\phi_1) \\ x_2(t)=e^{-\alpha_1\cdot t}\cdot X_1\cdot\sin(\zeta_1\cdot t+\rho_1)+e^{-\alpha_2\cdot t}\cdot X_2\cdot\sin(\zeta_2\cdot t+\rho_2)+T_2\cdot\sin(\omega\cdot t+\phi_2) \end{cases} \tag{66}$$

where the parameters α_i, X_i, ζ_i, ρ_i, T_i, ϕ_i ($i \in \{1, 2\}$) are defined as follows: $\alpha_i = p_{i1}$, $X_i = \text{sqrt}(A_i^2 + B_i^2)$, $\zeta_i = p_{i2}$, $\rho_i = \text{atan}(A_i/B_i)$, $T_i = \text{sqrt}(A'_i{}^2 + B'_i{}^2)$, and $\phi_i = \text{atan}(B'_i/A'_i)$.

The parameters A'_i and B'_i are obtained by solving the following linear system of equations:

$$\begin{bmatrix} \mathbf{M_{11}} & \mathbf{M_{12}} \\ \mathbf{M_{21}} & \mathbf{M_{22}} \end{bmatrix}\cdot\begin{bmatrix} {A'}_1 \\ {B'}_1 \\ {A'}_2 \\ {B'}_2 \end{bmatrix}=\begin{bmatrix} F\cdot k_2 \\ F\cdot b_2\cdot\omega \\ F\cdot\left(k_{eq_1}-\omega^2\cdot b_2\right) \\ F\cdot b_{eq_1}\cdot\omega \end{bmatrix} \tag{67}$$

where the matrix components are defined as:

$$\mathbf{M_{11}}=\begin{bmatrix} k_{eq_1}-\omega^2\cdot m_1 & -\omega\cdot b_{eq_1} \\ \omega\cdot b_{eq_1} & k_{eq_1}-\omega^2\cdot m_1 \end{bmatrix}\ \mathbf{M_{12}}=\begin{bmatrix} k_2 & \omega\cdot b_2 \\ -\omega\cdot b_2 & -k_2 \end{bmatrix} \\ \mathbf{M_{21}}=\begin{bmatrix} -k_2 & \omega\cdot b_2 \\ -b_2 & -k_2 \end{bmatrix}\ \mathbf{M_{22}}=\begin{bmatrix} k_{eq_2}-\omega^2\cdot m_2 & -\omega\cdot b_{eq_2} \\ \omega\cdot b_{eq_2} & k_{eq_2}-\omega^2\cdot m_2 \end{bmatrix} \tag{68}$$

The constants p_{i1} and p_{i2} correspond to the roots of the characteristic equation derived from the D operator method (similar to the 1-DoF case). The characteristic roots are defined as:

$$\begin{cases} D_{1,2}=-p_{11}\pm j\cdot p_{12} \\ D_{3,4}=-p_{21}\pm j\cdot p_{22} \end{cases} \tag{69}$$

Since the expressions for p_{i1} and p_{i2} are lengthy, they are referenced from previous calculations rather than explicitly stated.

The coefficients A_i and B_i are defined as:

$$\begin{cases} A_1 = C_{11} + C_{12}, & B_1 = \mathrm{j} \cdot (C_{11} - C_{12}) \\ A_2 = C_{13} + C_{14}, & B_2 = \mathrm{j} \cdot (C_{13} - C_{14}) \end{cases} \tag{70}$$

where C_{1n} ($n \in \{1, 2, 3, 4\}$) are integration constants determined based on the initial conditions of the system.

Some observations can be drawn from the latter results, for instance:

- The general solutions for $x_1(t)$ and $x_2(t)$ include transient components (exponentially decaying terms) and steady-state components (sinusoidal forcing terms).
- The constants p_{i1} and p_{i2} describe the damping and oscillatory behavior of the system.
- The matrix equation (68) provides the steady-state amplitude and phase shift for the system's response.
- This methodology can be extended to higher degrees of freedom systems (i.e., 3-DoF).

This analysis provides valuable insight into the coupled vibrational behavior of a two-mass system, crucial for engineering applications such as structural dynamics, automotive suspensions, and mechanical oscillators.

5.4 Solution for 2-DoF in dq coordinates

The model in dq coordinates is defined in (23). By following the same solution methodology applied in subsection 5.2 (which includes solving the homogeneous and particular solutions), the general solutions for the state variables $q_{ij}(t)$, where $i \in \{1, 2, 3, 4\}$ and $j \in \{\mathrm{d}, \mathrm{q}\}$, are expressed as:

$$q_{i_j}(t) = \sum_{i=1}^{4} \left[\mathrm{e}^{-\alpha_{i_{\mathrm{dq}}} \cdot t} \cdot X_{i_{\mathrm{dq}}} \cdot \sin\left(\zeta_{i_{\mathrm{dq}}} \cdot t + \rho_{i_{\mathrm{dq}}}\right) + \frac{\frac{k_i}{d}}{\prod_{i=0}^{4} (p_{i1}{}^2 + p_{i2}{}^2)} \right] \tag{71}$$

The solutions for D (eigenvalues of the system matrix) are given by:

$$\begin{cases} D_{1,2} = -p_{11} \pm \mathrm{j} \cdot p_{12} \\ D_{3,4} = -p_{21} \pm \mathrm{j} \cdot p_{22} \\ D_{5,6} = -p_{31} \pm \mathrm{j} \cdot p_{32} \\ D_{7,8} = -p_{41} \pm \mathrm{j} \cdot p_{42} \end{cases} \tag{72}$$

These roots represent the damping and oscillatory components of the system in the dq reference frame. Some parameter definition:

- Damping component: $\alpha_{i\mathrm{dq}} = \Re_{\mathrm{e}}\{D_n\}$, (real part of D_n).
- Oscillatory component: $\zeta_{i\mathrm{dq}} = \Im_{\mathrm{m}}\{D_n\}$, (imaginary part of D_n), where $n \in \{1, 3, 5, 7\}$.
- Phase shift: $\rho_i = \mathrm{atan}(A_i/B_i)$.
- Amplitude component: $X_{i\mathrm{dq}} = \mathrm{sqrt}(A_i^2 + B_i^2)$.

The coefficients A_i and B_i are expressed as: $A_i = C_{1h} + C_{1(h+1)}$ and $B_i = C_{1h} - C_{1(h+1)}$, where $h \in \{1, 2, 3, 4, 5, 6, 7, 8\}$, and C_{1h} represents integration constants derived from the system's initial conditions.

From the latter, it is possible to state that:

- The general solutions for $q_{ij}(t)$ contain transient (exponentially decaying) and steady-state (sinusoidal response) components.
- The eigenvalues D_n determine damping and oscillatory frequencies.
- The amplitude and phase shift are determined using $X_{i\mathrm{dq}}$ and ρ_i.
- The results validate that the dq-transformed system preserves the original system's linearity and oscillatory nature.

This approach provides a comprehensive mathematical framework to analyze mechanical vibration systems in dq coordinates, enabling control, optimization, and predictive maintenance applications in engineering.

5.5 Solution for 3-DoF in mechanical coordinates

The EoMs governing the 3-DoF system in mechanical coordinates are given by:

$$\begin{cases} m_1 \cdot \ddot{x}_1(t) + b_{\mathrm{eq}_1} \cdot \dot{x}_1(t) + k_{\mathrm{eq}_1} \cdot x_1(t) - b_2 \cdot \dot{x}_2(t) - k_2 \cdot x_2(t) = 0 \\ m_2 \cdot \ddot{x}_2(t) + b_{\mathrm{eq}_2} \cdot \dot{x}_2(t) + k_{\mathrm{eq}_2} \cdot x_2(t) - b_2 \cdot \dot{x}_1(t) - k_2 \cdot x_1(t) = 0 \\ m_3 \cdot \ddot{x}_3(t) + b_{\mathrm{eq}_3} \cdot \dot{x}_3(t) + k_{\mathrm{eq}_3} \cdot x_3(t) - b_3 \cdot \dot{x}_2(t) - k_3 \cdot x_2(t) = F \cdot \sin(\omega \cdot t) \end{cases} \quad (73)$$

The solutions for the displacement variables $x_1(t)$, $x_2(t)$, $x_3(t)$ in mechanical coordinates are obtained as follows in (74). This solution consists of two parts:

$$\begin{cases} x_1(t) = \mathrm{e}^{-\alpha_1 \cdot t} \cdot X_1 \cdot \sin(\zeta_1 \cdot t + \rho_1)\, \mathrm{e}^{-\alpha_2 \cdot t} \cdot X_2 \cdot \sin(\zeta_2 \cdot t + \rho_2) + \mathrm{e}^{-\alpha_3 \cdot t} \cdot X_3 \cdot \sin(\zeta_3 \cdot t + \rho_3) + \\ \qquad + T_1 \cdot \sin(\omega \cdot t + \phi_1) \\ x_2(t) = \mathrm{e}^{-\alpha_1 \cdot t} \cdot X_1 \cdot \sin(\zeta_1 \cdot t + \rho_1) + \mathrm{e}^{-\alpha_2 \cdot t} \cdot X_2 \cdot \sin(\zeta_2 \cdot t + \rho_2) + \mathrm{e}^{-\alpha_3 \cdot t} \cdot X_3 \cdot \sin(\zeta_3 \cdot t + \rho_3) + \\ \qquad + T_2 \cdot \sin(\omega \cdot t + \phi_2) \\ x_3(t) = \mathrm{e}^{-\alpha_1 \cdot t} \cdot X_1 \cdot \sin(\zeta_1 \cdot t + \rho_1) + \mathrm{e}^{-\alpha_2 \cdot t} \cdot X_2 \cdot \sin(\zeta_2 \cdot t + \rho_2) + \mathrm{e}^{-\alpha_3 \cdot t} \cdot X_3 \cdot \sin(\zeta_3 \cdot t + \rho_3) + \\ \qquad + T_3 \cdot \sin(\omega \cdot t + \phi_3) \end{cases} \quad (74)$$

1. Transient response: $\mathrm{e}^{-\alpha_i \cdot t} \cdot X_i \cdot \sin(\zeta_i \cdot t + \rho_i)$, which represents the natural oscillations that decay over time.
2. Steady-state response: $T_i \cdot \sin(\omega \cdot t + \phi_i)$, which is the forced response due to the external excitation.

Some parameters definition:

- Amplitude componets: $X_i = \mathrm{sqrt}(A_i^2 + B_i^2)$
- Phase shifts: $\rho_i = \mathrm{atan}(A_i/B_i)$, where $i \in \{1, 2, 3\}$.
- Definition of A_i and B_i: $A_1 = C_{11} + C_{12}$, $B_1 = \mathrm{j} \cdot (C_{11} - C_{12})$, $A_2 = C_{13} + C_{14}$, $B_2 = \mathrm{j} \cdot (C_{13} - C_{14})$, $A_3 = C_{15} + C_{16}$, and $B_3 = \mathrm{j} \cdot (C_{15} - C_{16})$, where C_{1n} ($n \in \{1, 2, 3, 4, 5, 6\}$) are integration constants determined by the initial conditions.
- Steady-state response parameters: $T_i = \mathrm{sqrt}(A'_i{}^2 + B'_i{}^2)$ and $\phi_i = \mathrm{atan}(B'_i/A'_i)$, where A'_i and B'_i are determined by solving a system of equations, which is too lengthy to be explicitly included.

To solve for the homogeneous solution, the characteristic equation is analyzed:

$$\begin{cases} D_{1,2} = -p_{11} \pm \mathrm{j} \cdot p_{12} \\ D_{3,4} = -p_{21} \pm \mathrm{j} \cdot p_{22} \\ D_{5,5} = -p_{31} \pm \mathrm{j} \cdot p_{32} \end{cases} \quad (75)$$

Some parameter definition:

- Damping component: $\alpha_i = \Re_{\mathrm{e}}\{D_n\}$.
- Oscillatory frequency component: $\zeta_i = \Im_{\mathrm{m}}\{D_n\}$, where $n \in \{1, 3, 5\}$.

From here, it can be seen that:

- The 3-DoF system exhibits three natural oscillatory modes, each with distinct frequencies ζ_i and decay rates α_i.
- The forced response depends on the excitation frequency ω and results in a steady-state oscillation with amplitudes T_i and phase shifts ϕ_i.
- The eigenvalues D_n characterize the dynamical behavior and are obtained from the system's characteristic equation.
- The integration constants C_{1n} must be calculated from the initial conditions.

This analytical framework allows to predict vibrational behavior, optimize system parameters, and design effective damping and control strategies.

5.6 Solution for 3-DoF in dq coordinates

The 3-DoF system in dq coordinates is represented by the state-space model defined in:

$$q_{i_j}(t) = \sum_{i=1}^{5} \left[\mathrm{e}^{-\alpha_{i_{\mathrm{dq}}} \cdot t} \cdot X_{i_{\mathrm{dq}}} \cdot \sin\left(\zeta_{i_{\mathrm{dq}}} \cdot t + \rho_{i_{\mathrm{dq}}}\right) + \frac{\frac{k_i}{d}}{\prod_{i=0}^{5} (p_{i1}{}^2 + p_{i2}{}^2)} \right] \quad (76)$$

where $i \in \{1, 2, 3, 4, 5\}$ and $j \in \{\mathrm{d}, \mathrm{q}\}$.

To solve the system, the characteristic equation is analyzed and determine its roots, denoted as D_n:

$$\begin{cases} D_{1,2} = -p_{11} \pm \mathrm{j} \cdot p_{12}, & D_{3,4} = -p_{21} \pm \mathrm{j} \cdot p_{22} \\ D_{5,6} = -p_{31} \pm \mathrm{j} \cdot p_{32}, & D_{7,8} = -p_{41} \pm \mathrm{j} \cdot p_{42} \\ D_{9,10} = -p_{51} \pm \mathrm{j} \cdot p_{52} \end{cases} \quad (77)$$

From these solutions:

- Damping component: $\alpha_{idq} = \Re_e\{D_n\}$.
- Oscillatory frequency component: $\zeta_{idq} = \Im_m\{D_n\}$, where $n \in \{1, 3, 5, 7, 9\}$.
- Phase shift: $\rho_i = \mathrm{atan}(A_i/B_i)$.
- Amplitude component: $X_{idq} = \mathrm{sqrt}(A_i^2 + B_i^2)$.

The constants A_i and B_i are defined as: $A_i = C_{1h} + C_{1(h+1)}$, $B_i = C_{1h} - C_{1(h+1)}$, where $h \in \{1, 2, 3, 4, 5, 6, 7, 8, 9, 10\}$.

From the mathematical modeling and solution approach, three fundamental insights emerge:

1. Scalability of the solution to higher-order systems:
    a. The solution approach for vibrational systems in both mechanical and dq coordinates is fully linear.
    b. As a result, the same methodology can be applied to higher-degree-of-freedom (n-DoF) systems, making it extendable and generalizable.
2. Distinct components in mechanical coordinates:
    a. The solutions for mechanical coordinate systems exhibit two primary components:
        - Transient vibration: This occurs due to the initial displacement from the equilibrium position and results in decaying oscillations.
        - Forced vibration: This occurs due to the external excitation force $f(t) = F \cdot \sin(\omega \cdot t)$. The system resonates at its natural frequency while also following the external frequency.
    b. This duality in vibration is well established in vibrational mechanics and is a key characteristic of oscillatory systems [44], [45].
3. Distinct components in dq coordinates:
    a. Unlike mechanical coordinates, the solutions in dq coordinates consist of:
        - A transient component, which exhibits exponential decay over time.
        - A constant steady-state component, which remains invariant over time.
    b. This is a defining characteristic of systems modeled in dq coordinates, as the transformation converts time-varying system variables into steady-state quantities in the dq domain [25], [27]–[29].

6.0 SIMULATION RESULTS

This section provides an in-depth examination of simulation results for the proposed 1-, 2-, and 3- DoF vibrational systems in both mechanical and dq coordinate domains. All simulations were conducted under the influence of a sinusoidal excitation force with a peak amplitude of 900 N and a linear frequency of 10 kHz. Table 1 summarizes the simulation parameters for each system, ensuring consistent initial conditions where: $x_{i0}(t) = \mathrm{d}x_{i0}(t)/\mathrm{d}t = 0$ for $i \in \{1, 2, 3\}$. The simulations were implemented using MATLAB-Simulink.

The simulation results for the 1-DoF system in mechanical coordinates are presented in **Figure 6**, which provides a comprehensive visualization of its dynamic behavior:

Table 1. Parameters of 1-, 2-, and 3-DoF system

System	Parameters	Values
1-DoF	k_1	10 [N/m]
	k_2	1 [N/m]
	b_1	$10 \cdot 10^{-1}$ [N-s/m]
	b_2	1.5 [N-s/m]
	m_1	100 [kg]
2-DoF	k_1	10 [N/m]
	k_2	1 [N/m]

	k_3	1.1 [N/m]
	b_1	10 [N-s/m]
	b_2	11 [N-s/m]
	b_3	1 [N-s/m]
	m_1	100 [kg]
	m_2	100 [kg]
3-DoF	k_1	10 [N/m]
	k_2	1 [N/m]
	k_3	11 [N/m]
	k_4	1.1 [N/m]
	b_1	1 [N-s/m]
	b_2	$1.1 \cdot 10^{-5}$ [N-s/m]
	b_3	$1. \cdot 10^{-6}$ [N-s/m]
	b_4	$10 \cdot 10^{-6}$ [N-s/m]
	m_1	100 [kg]
	m_2	100 [kg]
	m_3	100 [kg]

- **Figure 6(a)** and **(b):** Depict the position variable $x_1(t)$ and velocity variable $dx_1(t)/dt$.
- **Figure 6(c)** and **(d):** Show zoomed-in views to highlight key dynamic characteristics.
- **Figure 6(d):** Represents the excitation force $f_1(t)$.

From **Figure 6(a)**, the forced vibration component exhibits a smaller amplitude than the free vibration component, consistent with the expression derived in (50), where: $T << X$.

Analyzing **Figure 6(b)**, the velocity equation: $\dot{x}_1(t) = \sqrt{\alpha^2 + \zeta^2} \cdot X \cdot e^{-\alpha \cdot t} \cdot \cos\left(\zeta \cdot t + \rho + \tan^{-1}\left(\frac{\alpha}{\zeta}\right)\right) + \omega \cdot T \cdot \cos(\omega \cdot t + \phi)$ reveals the transient and steady-state components. The natural frequency is approximately $\zeta \approx 0.323$ rad/s, while the forced vibration frequency corresponds to $\omega \approx 62.832 \times 10^3$ rad/s.

The transient response in dq coordinates is depicted in **Figure 7**, illustrating the dynamics of:

- $q_{1d}(t)$ and $q_{1q}(t)$.
- $q_{2d}(t)$ and $q_{2q}(t)$.
- $f_{1d}(t)$ and $f_{1q}(t)$.

Some key observations can be drawn from the latter, for instasnce:

- The transient component follows a cosine waveform, while the steady-state component remains constant, confirming the validity of expressions (61)–(64).
- The excitation force conversion in dq coordinates results in:
  - $f_{1d}(t)$ = 0 N (d-axis component).
  - $f_{1q}(t)$ = 900 N (q-axis component).

Table 2 summarizes the steady-state values of $q_{nm}(t)$, where $n \in \{1, 2\}$ and $m \in \{d, q\}$.

The transient dynamics for the 2-DoF system in mechanical coordinates are illustrated in **Figure 8**, showing the responses of $x_1(t)$, $x_2(t)$, and their derivatives. Notable observations include:

- **Figure 8(a):** Confirms the expected dynamic response of $x_1(t)$.
- The presence of two distinct frequency components in the transient state, corresponding to (66).
- **Figure 8(d):** Highlights a beating effect, a well-documented phenomenon in vibrational systems [44], [45].
- The displacement $x_2(t)$ exhibits:
  - A low-frequency component at 1.31 mHz (natural frequency).
  - A high-frequency component at 10 kHz, originating from $f_1(t)$.

The dq transformation results for the 2-DoF system are presented in **Figure 9**, showcasing variables: $q_{mn}(t)$, where $m \in \{1, 2, 3, 4\}$ and $n \in \{d, q\}$. Some key insights:

- Transient and steady-state components confirm the validity of (71).
- Table 3 shows that steady-state values are close to zero, indicating effective transformation.

The dynamic behavior of the 3-DoF system in mechanical coordinates is shown in **Figure 10**, depicting variables: $x_i(t)$ and $dx_i(t)/dt$ for $i \in \{1, 2, 3\}$.

Some observations:

- **Figure 10(a):** Confirms the expected transient and steady-state dynamics of $x_1(t)$.

Figures 10(e) and **(f):** Highlight the response of $dx_3(t)/dt$ under external excitation.

The dq-domain responses for the 3-DoF system are illustrated in Figure 11, focusing on: $q_{mn}(t)$ where $m \in \{1, 2, 3, 4,$

Table 2. 1-DoF steady-state values of $q_{nm}(t)\ \forall\ m \in \{1, 2\}$ and $n \in \{1, 2\}$

Parameters	Values
$q_{1d}(t)$	~0 [m]
$q_{1q}(t)$	$-2.28 \cdot 10^{-9}$ [m]
$q_{2d}(t)$	$1.432 \cdot 10^{-4}$ [m/s]
$q_{2q}(t)$	~0 [m/s]

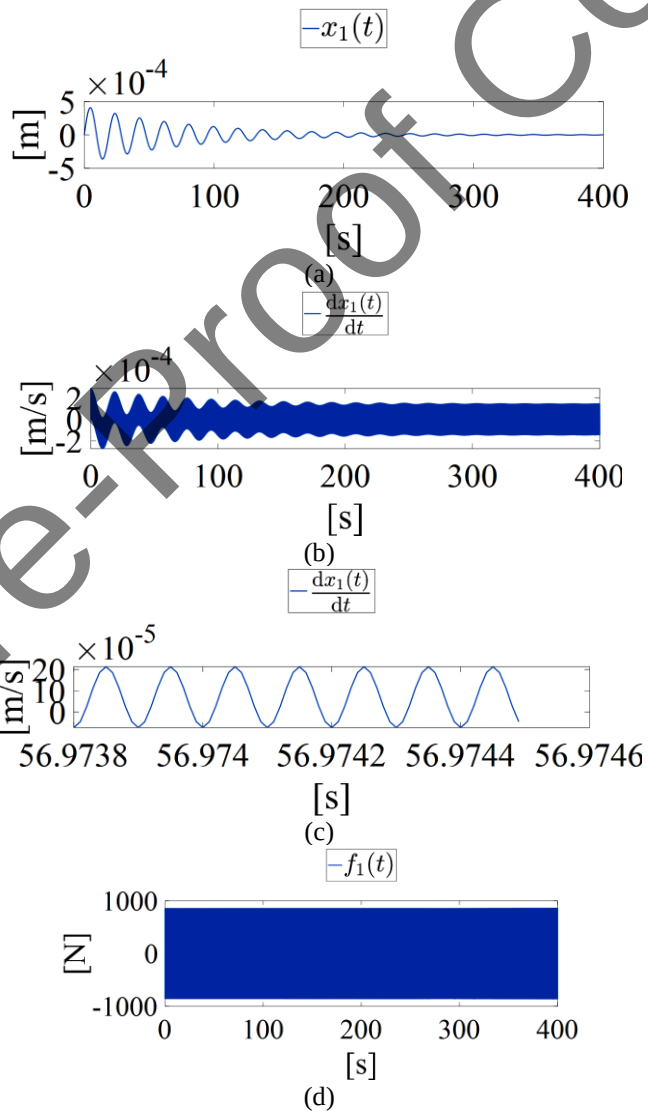

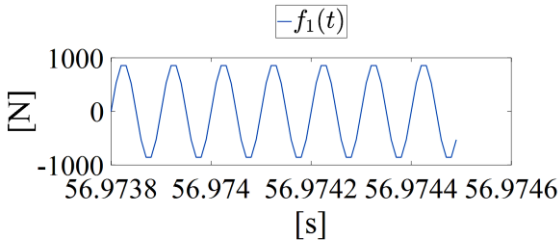

(e)

Figure 6. Transient simulation results of the 1-DoF system in mechanical coordinates. Initial conditions $x_{10}(t) = dx_{10}(t)/dt = 0$. (a) Dynamics of $x_1(t)$. (b) Dynamics of $dx_1(t)/dt$. (c) Zoomed view of $x_1(t)$. (d) Dynamics of $f_1(t)$. (e) Zoomed view of $f_1(t)$

5, 6} and $n \in$ {d, q}.

- Two components (transient and steady-state) align with (76).
- Table 4 confirms negligible steady-state magnitudes of $q_{mn}(t)$.

This study systematically analyzes 1-, 2-, and 3-DoF vibrational systems under sinusoidal excitation, drawing three major conclusions:

1. dq coordinates simplify analysis and control:
    a. In mechanical coordinates, the oscillatory response contains multiple frequency components.
    b. dq transformation simplifies the system to steady-state dc variables, improving control and stability.
2. Multi-DoF systems exhibit beating and multi-frequency effects:

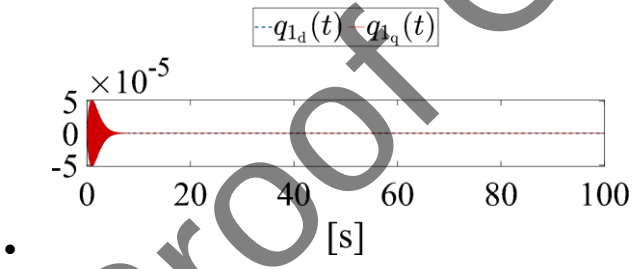

(a)

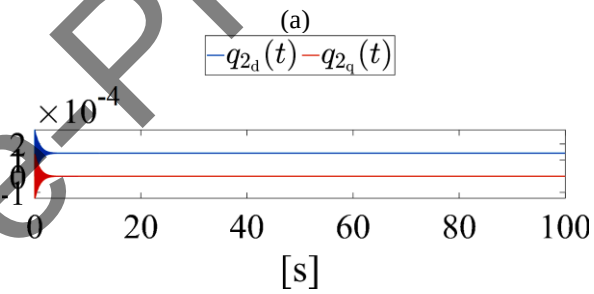

(b)

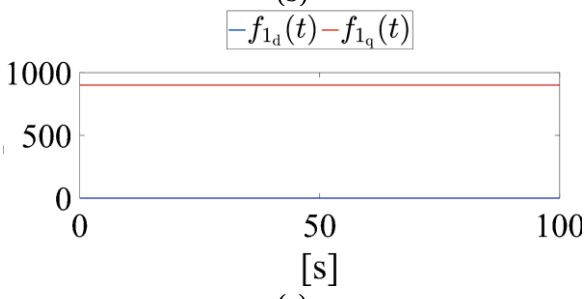

(c)

Figure 7. Transient simulation results of the 1-DoF system in dq coordinates. Initial conditions $q_{mn}(t) = 0$ where $m \in$ {1, 2} and $n \in$ {d, q}. (a) Dynamics of $q_{1d}(t)$ and $q_{1q}(t)$. (b) Dynamics of $q_{1d}(t)$ and $q_{1q}(t)$. (c) Dynamics of $f_{1d}(t)$ and $f_{1q}(t)$

Table 3. 2-DoF Steady-state values of $q_{nm}(t)$ $\forall$ $m \in$ {1, 2, 3, 4} and $n \in$ {d, q}

Parameters	Values
$q_{1d}(t)$	~0 [m]

$q_{1q}(t)$	~0 [m]
$q_{2d}(t)$	~0 [m/s]
$q_{2q}(t)$	~0 [m/s]
$q_{3d}(t)$	~0 [m/s]
$q_{3q}(t)$	~0 [m/s]
$q_{4d}(t)$	$1.432 \cdot 10^{-4}$ [m/s]
$q_{4q}(t)$	~0 [m/s]

Table 4. 3-DoF Steady-state values of q_{nm}(t) $\forall$ $m \in \{1, 2, 3, 4, 5, 6\}$ and $n \in \{d, q\}$

Parameters	Values	Parameters	Values
$q_{1d}(t)$	~0 [m]	$q_{4d}(t)$	~0 [m/s]
$q_{1q}(t)$	~0 [m]	$q_{4q}(t)$	~0 [m/s]
$q_{2d}(t)$	~0 [m/s]	$q_{5d}(t)$	~0 [m/s]
$q_{2q}(t)$	~0 [m/s]	$q_{5q}(t)$	$-2.28 \cdot 10^{-9}$ [m]
$q_{3d}(t)$	~0 [m/s]	$q_{6d}(t)$	$1.432 \cdot 10^{-4}$ [m/s]
$q_{3q}(t)$	~0 [m/s]	$q_{6q}(t)$	~0 [m/s]

a. The 2-DoF system exhibits beating phenomena due to multi-frequency interactions.

b. The 3-DoF system contains two primary frequency components, illustrating complex vibrational interactions.

dq transformation enhances convergence and control design:

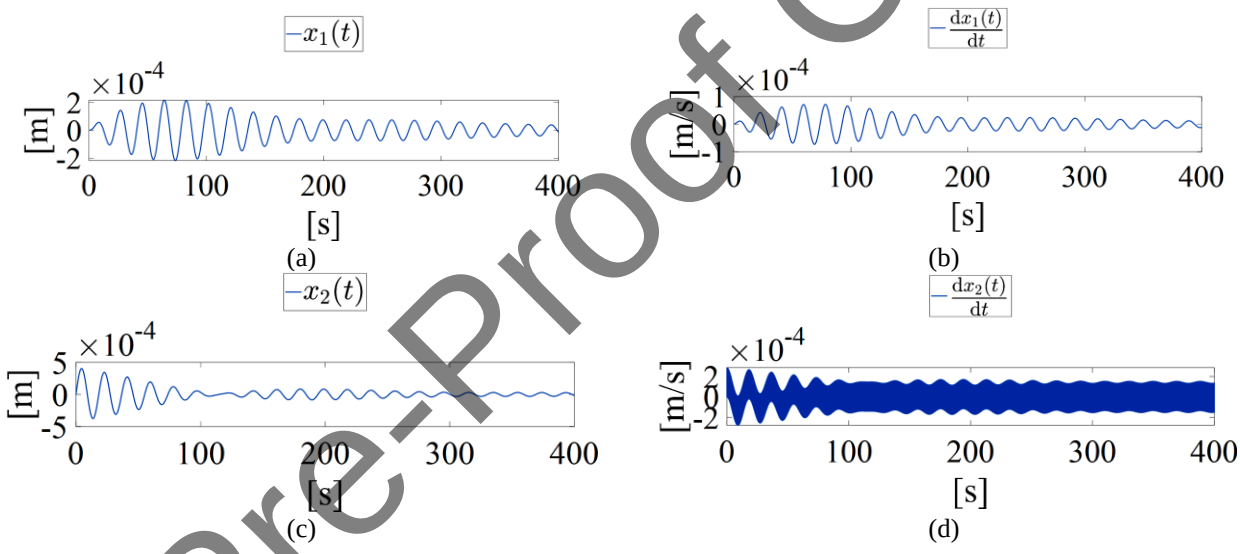

Figure 8. Transient simulation results of the 2-DoF system in mechanical coordinates. Initial conditions $x_{i0}(t) = dx_{i0}(t)/dt = 0$ where $i \in \{1, 2\}$. (a) Dynamics of $x_1(t)$. (b) Dynamics of $dx_1(t)/dt$. (c) Dynamics of $x_2(t)$. (d) Dynamics of $dx_2(t)/dt$

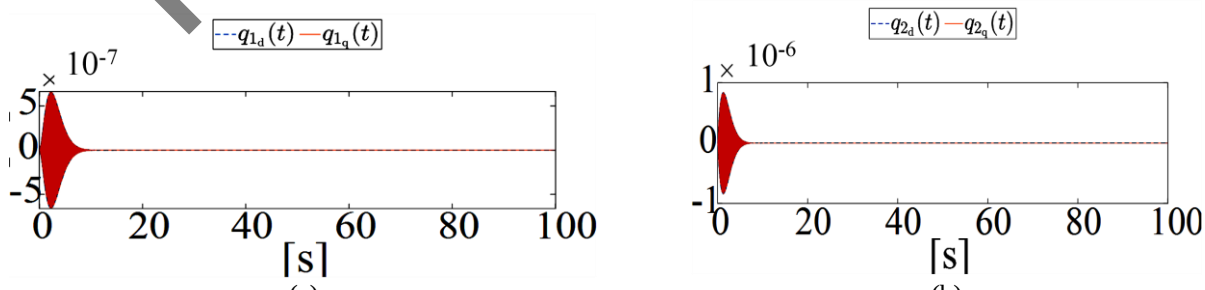

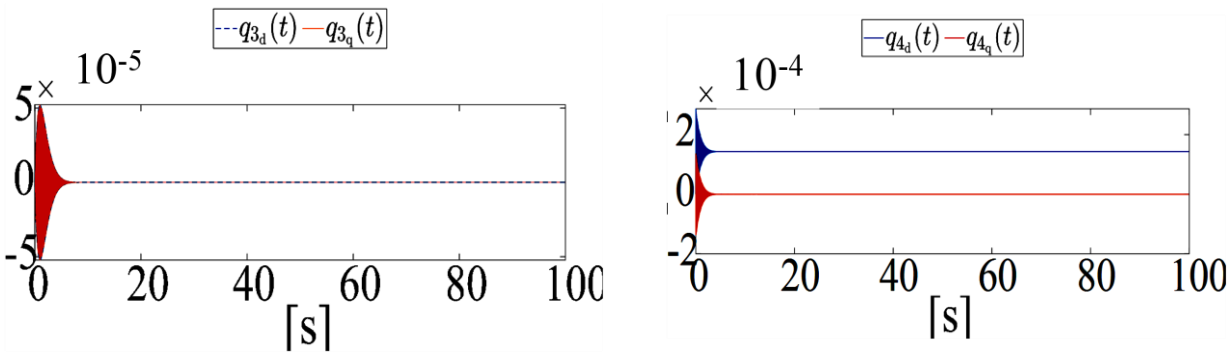

(c) (d)

Figure 9. Transient simulation results of the 2-DoF system in dq coordinates. Initial conditions $q_{mn}(t) = 0$ where $m \in \{1, 2, 3, 4\}$ and $n \in \{d, q\}$. (a) Dynamics of $q_{1d}(t)$ and $q_{1q}(t)$. (b) Dynamics of $q_{2d}(t)$ and $q_{2q}(t)$. (c) Dynamics of $q_{3d}(t)$ and $q_{3q}(t)$. (d) Dynamics of $q_{4d}(t)$ and $q_{4q}(t)$

a. Faster convergence to steady-state conditions is observed in dq coordinates.

b. dq transformation facilitates the design of linear compensators by transforming ac signals into dc equivalents.

Finally, this work attempts to show the effectiveness of dq transformation in vibrational mechanics, particularly for multi-DoF systems. Future research can further explore linear compensator design and experimental validation of dq-based control strategies for complex vibrational systems.

7.0 CONCLUSION

Through a comprehensive simulation study and analysis of 1-, 2-, and 3-DoF vibrational systems under sinusoidal excitation, this research provides valuable insights into system dynamics and the advantages of the dq transformation in vibrational mechanics. The study highlights the transformation's effectiveness in simplifying dynamic analysis, improving control strategies, and facilitating steady-state convergence in complex mechanical systems.

The 1-DoF system, characterized by low damping, exhibits a distinct oscillatory pattern composed of two frequency

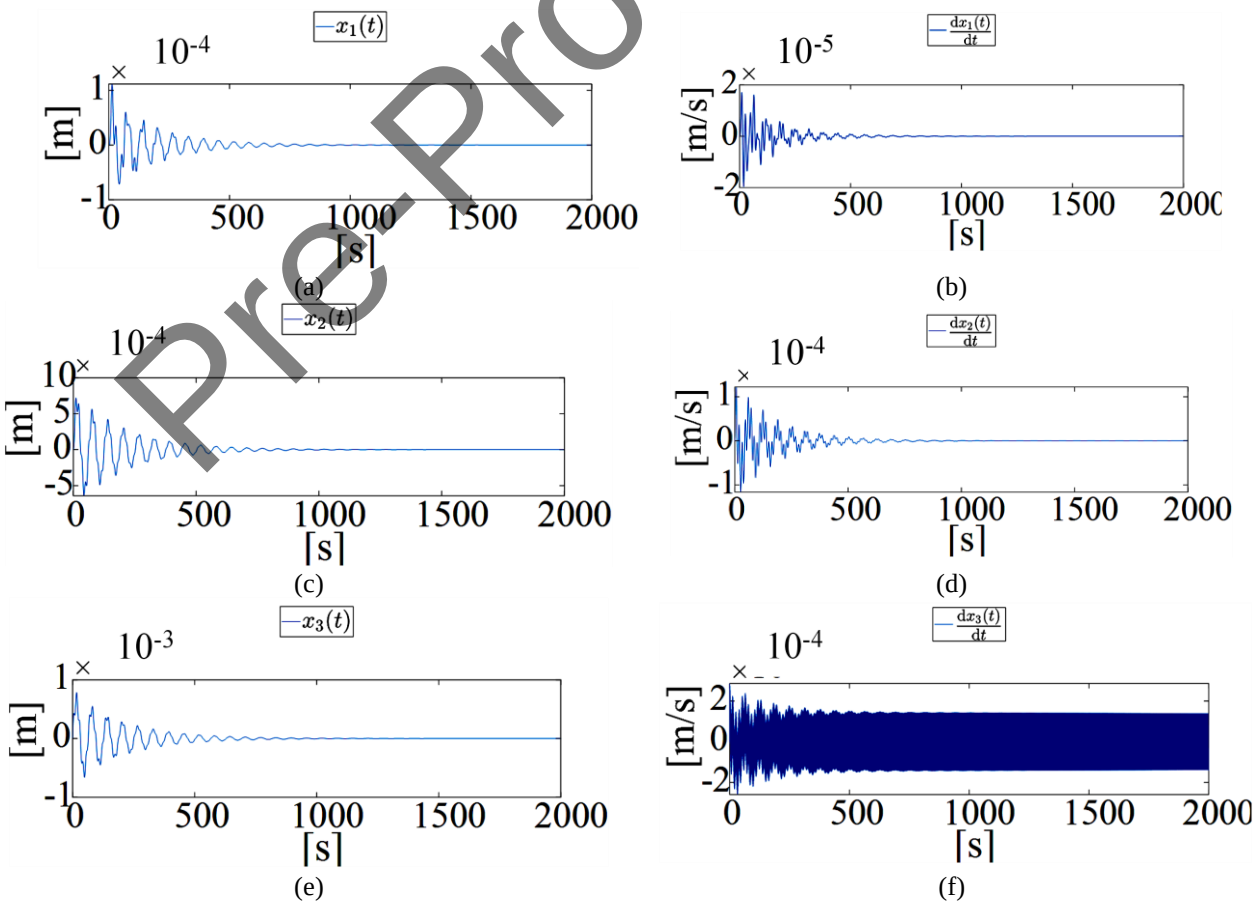

(a) (b)

(c) (d)

(e) (f)

Figure 10. Transient simulation results of the 3-DoF system in mechanical coordinates. Initial conditions $x_{i0}(t) = \mathrm{d}x_{i0}(t)/\mathrm{d}t = 0$ for $i \in \{1, 2, 3\}$. (a) Dynamics of $x_1(t)$. (b) Dynamics of $\mathrm{d}x_1(t)/\mathrm{d}t$. (c) Dynamics of $x_2(t)$. (d) Dynamics of $\mathrm{d}x_2(t)/\mathrm{d}t$. (e) Dynamics of $x_3(t)$. (f) Dynamics of $\mathrm{d}x_3(t)/\mathrm{d}t$

components. The application of the dq transformation offers a strategic reduction in system complexity, effectively decoupling system dynamics and providing a clearer understanding of steady-state behavior. This transformation improves the response characteristics of the system, particularly in control applications, where it aids in stability enhancement and performance optimization.

Moving to the 2-DoF system, a higher degree of complexity emerges in mechanical coordinates, as interactions

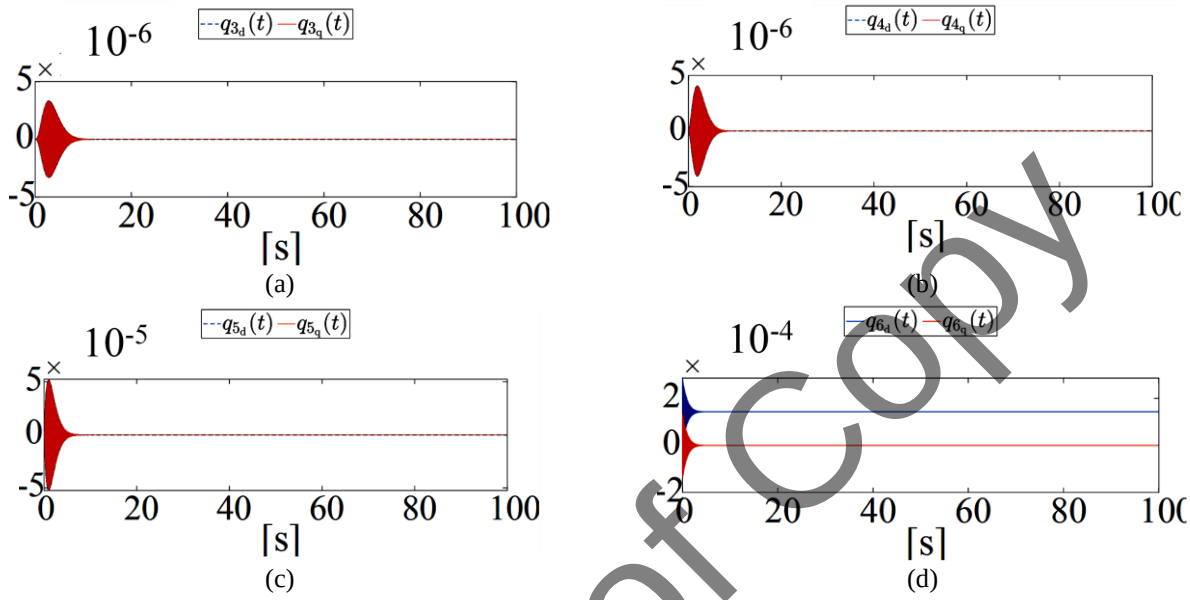

Figure 11. Transient simulation results of the 3-DoF system in dq coordinates. Initial conditions $q_{mn}(t) = 0$ where $m \in \{1, 2, 3, 4, 5, 6\}$ and $n \in \{\mathrm{d}, \mathrm{q}\}$. (a) Dynamics of $q_{1\mathrm{d}}(t)$ and $q_{1\mathrm{q}}(t)$. (b) Dynamics of $q_{2\mathrm{d}}(t)$ and $q_{2\mathrm{q}}(t)$. (c) Dynamics of $q_{3\mathrm{d}}(t)$ and $q_{3\mathrm{q}}(t)$. (e) Dynamics of $q_{5\mathrm{d}}(t)$ and $q_{5\mathrm{q}}(t)$. (f) Dynamics of $q_{6\mathrm{d}}(t)$ and $q_{6\mathrm{q}}(t)$

between masses result in beating effects and multi-frequency oscillations. The dq transformation decouples complex frequency behaviors, making it easier to analyze system responses. It also reveals the minimal influence of masses not directly subjected to external excitation and streamlines control implementation, demonstrating its practicality for complex mechanical systems. This study underscores how dq analysis enhances the understanding of multi-DoF systems, particularly when investigating energy interactions and resonance effects.

The 3-DoF system further demonstrates the effectiveness of the dq transformation in analyzing external force influences and understanding system interactions. Notably, the system contains dual frequency components, which are simplified through dq transformation. Additionally, the dq transformation converts ac signals into dc, facilitating linear compensator applications. This method ultimately improves system stability and enhances control performance. By reducing system complexity and allowing independent analysis of interacting components, the dq transformation provides significant advantages in vibrational system modeling and control.

The sinusoidal excitation used in this study directly influences system energy distributions, leading to complex interactions between oscillatory components. It also results in transient and steady-state behaviors, which are effectively decoupled in dq coordinates, providing a deeper understanding of energy transformations within multi-DoF systems. The results underscore the effectiveness of the dq transformation in providing a clear, structured framework for analyzing and optimizing dynamic responses in complex vibrational systems.

The findings of this study hold significant implications for advanced control systems, particularly in designing controllers for multi-DoF systems that require precise system behavior modeling. Furthermore, the dq transformation enhances stability and performance by simplifying control algorithms and facilitates real-time implementation of advanced controllers, where dq conversion minimizes computational complexity.

By demonstrating the advantages of dq transformation in vibrational mechanics, this research lays a foundation for future studies aimed at optimizing control strategies for nonlinear, multi-DoF systems. Additionally, it opens the door for exploring applications beyond mechanical systems, including power electronics, electrical machines, and robotics.

8.0 REFERENCES

[1] D. Findeisen, *System Dynamics and Mechanical Vibrations: An Introduction*. 2010.

[2] R. Arias, A. P. da Cunha, and A. R. Garcia Ramirez, "Teaching of mechanical vibration concepts using the computational simulation," *IEEE Latin America Transactions*, vol. 18, no. 04, pp. 659–667, Apr. 2020.
[3] E. A. Burda, G. V. Zusman, I. S. Kudryavtseva, and A. P. Naumenko, "An Overview of Vibration Analysis Techniques for the Fault Diagnostics of Rolling Bearings in Machinery," *Shock and Vibration*, vol. 2022, p. e6136231, Dec. 2022.
[4] H. P. Bloch and F. K. Geitner, Eds., "Chapter 5 - Vibration Analysis," in *Practical Machinery Management for Process Plants*, vol. 2, Gulf Professional Publishing, 1999, pp. 351–433.
[5] B. Yang, "Chapter 10 - Vibration analysis of one-degree-of-freedom systems," in *Stress, Strain, and Structural Dynamics (Second Edition)*, B. Yang, Ed. Academic Press, 2023, pp. 431–528.
[6] F. Svaricek, C. Bohn, P. Marienfeld, H.-J. Karkosch, T. Fueger, F. Svaricek, C. Bohn, P. Marienfeld, H.-J. Karkosch, and T. Fueger, "Automotive Applications of Active Vibration Control," in *Vibration Control*, IntechOpen, 2010.
[7] O. I. Vulcu and M. Arghir, "Impact of maintenance in the automotive field. Experimental study of mechanical vibration," *IOP Conf. Ser.: Mater. Sci. Eng.*, vol. 147, no. 1, p. 012056, Aug. 2016.
[8] Z. You, "Design of automotive mechanical automatic transmission system based on torsional vibration reduction," *Journal of Vibroengineering*, vol. 25, no. 4, pp. 683–697, Jun. 2023.
[9] M. Bonato and P. Goge, "Methods for analysis and comparison of automotive vibration tests," in *2016 Annual Reliability and Maintainability Symposium (RAMS)*, pp. 1–6, Jan. 2016.
[10] K. C. Panda, "Dealing with Noise and Vibration in Automotive Industry," *Procedia Engineering*, vol. 144, pp. 1167–1174, Jan. 2016.
[11] S. Jiang, H. Liu, Z. Gu, and Q. Liu, "Mechanical Simulation Analysis of Aerospace High Reliability Electronic Equipment," *J. Phys.: Conf. Ser.*, vol. 2187, no. 1, p. 012035, Feb. 2022.
[12] L. Liu and B. Tian, "Comprehensive Engineering Frequency Domain Analysis and Vibration Suppression of Flexible Aircraft Based on Active Disturbance Rejection Controller," *Sensors*, vol. 22, no. 16, p. 6207, Jan. 2022.
[13] B. A and S. Zolkiewski, "Dynamic analysis of the mechanical systems vibrating transversally in transportation," *Journal of Achievements in Materials and Manufacturing Engineering*, vol. 20, Jan. 2007.
[14] W. Wang, G. Shen, Y. Zhang, Z. Zhu, C. Li, and H. Lu, "Dynamic reliability analysis of mechanical system with wear and vibration failure modes," *Mechanism and Machine Theory*, vol. 163, p. 104385, Sep. 2021.
[15] K. Kamei and M. A. Khan, "Current challenges in modelling vibrational fatigue and fracture of structures: a review," *J Braz. Soc. Mech. Sci. Eng.*, vol. 43, no. 2, p. 77, Jan. 2021.
[16] M. Romanssini, P. C. C. de Aguirre, L. Compassi-Severo, and A. G. Girardi, "A Review on Vibration Monitoring Techniques for Predictive Maintenance of Rotating Machinery," *Eng*, vol. 4, no. 3, pp. 1797–1817, Sep. 2023.
[17] D. Y. Ou and C. M. Mak, "A Review of Prediction Methods for the Transient Vibration and Sound Radiation of Plates," *Journal of Low Frequency Noise, Vibration and Active Control*, vol. 32, no. 4, pp. 309–322, Dec. 2013.
[18] N. Anh and N. Nguyen, "Design of non-traditional dynamic vibration absorber for damped linear structures," *Proceedings of the Institution of Mechanical Engineers, Part C: Journal of Mechanical Engineering Science*, vol. 228, no. 1, pp. 45–55, Jan. 2014.
[19] M. H. Mohd Ghazali and W. Rahiman, "Vibration Analysis for Machine Monitoring and Diagnosis: A Systematic Review," *Shock and Vibration*, vol. 2021, p. e9469318, Sep. 2021.
[20] S. Saxena and M. Patel, "Evaluating dynamic behaviour of a concrete dam using modal analysis," *Materials Today: Proceedings*, vol. *93*, pp.296-301, 2023.
[21] H. Van der Auweraer, "Structural dynamics modeling using modal analysis: applications, trends and challenges," in *IMTC 2001. Proceedings of the 18th IEEE Instrumentation and Measurement Technology Conference. Rediscovering Measurement in the Age of Informatics (Cat. No.01CH 37188)*, vol. 3, pp. 1502–1509 vol.3, May 2001.
[22] K. Ogata, *Modern Control Engineering*, 5th edition. Boston: Pearson, 2009.
[23] B. C. Kuo, *Automatic control systems*, 6th edition. Englewood Cliffs, N.J: Prentice Hall, 1991.
[24] W. S. Levine, *The Control Handbook (three volume set)*. CRC Press, 2018.
[25] C. J. O'Rourke, M. M. Qasim, M. R. Overlin, and J. L. Kirtley Jr, "A Geometric Interpretation of Reference Frames and Transformations: dq0, Clarke, and Park," *Colm O'Rourke*, Dec. 2019.
[26] M. Gonzalez, V. Cardenas, and F. Pazos, "DQ transformation development for single-phase systems to compensate harmonic distortion and reactive power," in *9th IEEE International Power Electronics Congress, 2004. CIEP 2004*, pp. 177–182, Oct. 2004.
[27] M. F. Schonardie and D. C. Martins, "Application of the dq0 transformation in the three-phase grid-connected PV systems with active and reactive power control," in *2008 IEEE International Conference on Sustainable Energy Technologies*, pp. 18–23, Nov. 2008.
[28] K. S. Low, M. F. Rahman, and K. W. Lim, "The dq transformation and feedback linearization of a permanent magnet synchronous motor," in *Proceedings of 1995 International Conference on Power Electronics and Drive Systems. PEDS 95*, pp. 292–296 vol.1, Feb. 1995.
[29] S. W. L. Tobing, R. Afdila, P. E. Panjaitan, N. C. Situmeang, K. N. Hutagalung, and R. Sidabutar, "ABC to DQ Transformation for Three-Phase Inverter Design as Prime Mover Speed Control in Microgrid System," in *2022 6th International Conference on Electrical, Telecommunication and Computer Engineering (ELTICOM)*, pp. 70–74, Nov. 2022.
[30] M. F. Schonardie, R. F. Coelho, R. Schweitzer, and D. C. Martins, "Control of the active and reactive power using dq0 transformation in a three-phase grid-connected PV system," in *2012 IEEE International Symposium on Industrial Electronics*, pp. 264–269, May 2012.
[31] K. Abe, *The Clark and Park transformations: Coordinate transformations for Brushless DC motor in field-oriented control*. 2017.
[32] J. Campos Salazar, A. Viani-Abad, and R. Sandoval-García, "Modeling and Simulation of a Single-Phase Linear Multi-Winding Transformer in the d-q Frame," *Journal of Electronics and Electrical Engineering*, vol. 3, pp. 206–235, Jun. 2024.
[33] B. C. Trento, "Modeling and Control of Single Phase Grid-Tie Converters," *Masters Theses*, Aug. 2012.
[34] A. C. J. Luo, *Nonlinear Deformable-body Dynamics*, 2010th edition. Beijing : Berlin ; New York: Springer Verlag, 2010.
[35] A. W. Pila, *Introduction To Lagrangian Dynamics*, 1st ed. 2020 edition. Cham, Switzerland: Springer, 2019.

[36] G. A. Anastassiou and I. F. Iatan, "Linear Transformations," in *Intelligent Routines II: Solving Linear Algebra and Differential Geometry with Sage*, G. A. Anastassiou and I. F. Iatan, Eds. Cham: Springer International Publishing, 2014, pp. 91–134.
[37] W. Hauser, *Introduction to the Principles of Mechanics*. Addison-Wesley Publishing Company, 1965.
[38] B. Porter and R. Crossley, *Modal Control: Theory and Applications*, 0 edition. London: Taylor & Francis, 1972.
[39] K. Peleg, "Power and energy in mechanical systems," *International Journal of Mechanical Sciences*, vol. 29, no. 4, pp. 259–269, Jan. 1987.
[40] B. V. Malozyomov, N. V. Martyushev, S. N. Sorokova, E. A. Efremenkov, and M. Qi, "Mathematical Modeling of Mechanical Forces and Power Balance in Electromechanical Energy Converter," *Mathematics*, vol. 11, no. 10, p. 2394, Jan. 2023.
[41] M. R. Spiegel, *Spiegel: Applied Differential Equations*. Prentice-Hall, 1958.
[42] F. Ayres, *Schaum's Outline of Theory and Problems of Differential Equations*. McGraw-Hill, 1967.
[43] W. H. Hayt, J. E. Kemmerly, S. Durbin, and S. M. Durbin, *Engineering Circuit Analysis*. 2001.
[44] W. W. Seto, *Theory and problems of mechanical vibrations:*, First Edition. McGraw-Hill, 1964.
[45] W. W. Seto, *Theory and Problems of Acoustics*.